Chirality-Controlled Preparation and Single Molecule Characterisation of Carbon Nanotubes

Master's Thesis

Samaneh Mashaghi Tabari

Nanoscience Center
Department of Physics
Department of Biological and Environmental Science
University of Jyväskylä

Preface

The work presented in this master's thesis was done between September 2010 and June 2011 at Nanoscience Center at the Department of Physics in the University of Jyväskylä.

Jyväskylä, June 15, 2011

Samaneh Mashaghi Tabari

Abstract

Nanostructures have gained increasing attention not only for their basic scientific richness, but also because they promise novelties and potentials that may lead to technological revolution. Carbon nanotubes (CNT's) are one of the primary focuses of nanotechnology because of their unique physical properties such as huge Young modulus, high tensile strength, thermal and electrical conductivity. However many of their physical properties are extremely sensitive to their atomic structure. In order to optimize utilization of CNTs, their fundamental material properties should be well understood. A single shell of a CNT is composed of a wrapped up sheet of graphite. Depending on the wrapping, single wall carbon nanotubes (SWCNT) may have numerous different chiralities. Owing to SWCNT's outstanding mechanical and electrical properties, many of their fundamental studies and technological applications require a population of tubes with identical chiralities. Separating SWCNT of different chiralities from each other is, however, a challenging problem. One proposed solution is to construct DNA-SWCNT hybrid and separate SWCNTs by their chiralities and diameter chromatographically. An oligomer of specific sequence of single-stranded DNA (ssDNA) has been shown to wrap around a SWCNT of a specific chirality and form ssDNA-SWCNT hybrid. Additionally self assembled DNA-SWCNT hybrids can be used a unique platform to study nucleic acid folding structures and other biophysical properties.

In this study, DNA-SWCNT hybrids were produced and sorted according to the chirality of the CNT in a controlled fashion by ion exchange chromatography (IEX). During the chromatography, eluent were collected in a series of fractions whose composition was monitored by HPLC detector. Selected fractions were then subjected to detailed analysis by UV-Vis to prove that the single chirality purification of DNA-SWCNT was successful. For confirmation, Atomic Force Microscopy was conducted on the samples and DNA wrapped SWCNTs with expected diameter and DNA pitch were observed indicating that the spectral signatures recorded in UV-Vis analysis is indeed coming from sorted DNA-SWCNT.

In future DNA-SWCNT hybrids will be deposited on an advanced nanofabricated silicon chip containing tiny openings. TEM measurements including DNA supertwist imaging and CNT chirality investigations will be done for direct determination of chiral indices (n,m) of the SWCNTs from their electron diffraction patterns (EDPs).

Contents

List of Abbreviations

A	Adenine
AFM	Atomic force microscopy
C	Cytosine
CNT	Carbon nanotube
CVD	Chemical vapor depossition
DNA	Deoxyribonucleic acid
FET	field-effect transistor
G	Guanine
HiPCO	High pressure carbon monoxide
HPLC	High pressure liquid chromatography
IEX	Ion exchange chromatography
JDOS	Joint density function
MWCNT	Multi walled carbon nanotube
NEMS	nano-electromechanical systems
SEM	Scanning Electron Microscope
ssDNA	Single stranded DNA
SWCNT	Single walled carbon nanotube
T	Thymine
TEM	Transmission Electron Microscope

1. Introduction

Carbon nanotube (CNT) is a rather new man-made material with striking atomic and intriguing electronic structures. Single-walled carbon nanotubes (SWCNTs) have attracted special attention for their potential applications in drug delivery[1], biosensors[2] and nanoelectronics[3].

DNA is a natural material that carries genetic information in living cells. DNA has been attractive to researchers from different disciplines, due to its unique physical chemical properties and its central role in biology.

When exposed in solution, DNA forms a stable hybrid with CNTs by wrapping around them in a helical manner (see Figure 1).[4,5] The hybrid is a negatively charged colloidal rod that can be attracted to a surface with positive charge. The strength of the attractive force varies by the electronic properties of the carbon nanotube, allowing their separation. The construct can be used to disperse, sort[4,5] and pattern[6] nanotubes. Additionally it is proved useful for transportation of DNA into a cell, and for thermal ablation treatment.[7] Strength of dispersion, sorting efficiency, and stability in the cellular environment all depend on the interaction between DNA and a CNT.[8] From the standpoint of carbon nanotube manipulation, DNA−CNT hybrids provide a model system to address general questions on how polymers wrap around carbon nanotubes. Because DNA forms a novel structure in combination with CNTs, study of the hybrid may shed light on the behavior of DNA itself.
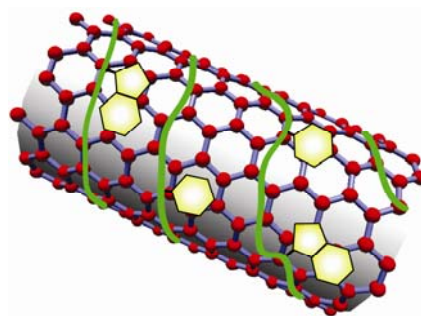
Figure 1 Schematic view of a ssDNA wrapped around a SWCNT.

In this thesis DNA was used as a powerful molecular tool to separate a synthetic mixture of SWCNTs into its components with a characteristic chirality. The strong interaction between single stranded DNA (ssDNA) and SWCNT have been used effectively for solution based CNT manipulation and Ion Exchange chromatography (IEX) separation of SWCNTs for application in nanoelectromechanical devices. In this current study, chirality separation of SWCNT has been characterized by UV-Vis spectroscopy and Atomic Force Microscopy.

2. Back ground

2.1 Carbon nanotube

The discovery of carbon nanotubes (CNT) dates back to 1976 when Endo[9] synthesized vapour-grown carbon fibres, however at the time it was left unnoticed and was not given any thought and focus.

It was only after Iijima's work in 1991[10] that global scientific attention was turned to these appealing carbon structures. Consequently intense studies on the properties, structure, and applications of these unique materials have been conducted.[11, 12]

2.1.1 Structure and Chirality of Carbon nanotubes

CNTs are carbon-based tubules with exceptionally high aspect ratio, located structurally between planar graphene/graphite layers and molecular fullerenes.

Carbon nanotubes can be categorized by their structures to single-wall nanotubes (SWCNT) and multi-wall nanotubes (MWCNT). A single walled carbon nanotube is structurally equivalent to a sheet of graphene rolled into a tube i.e. each carbon atom has three neighboring carbons, lying in the plane of the tube wall in a hexagonal arrangement. Such an arrangement leads to a minimum number of carbon dangling bonds since it has no edge sites compared to an equivalent graphene sheet. Multi-wall nanotubes can be seen in two forms, either in the form of a coaxial assembly of SWCNT or as a single sheet of graphite which is rolled like a scroll.

To determine the structure of a single walled carbon nanotube, it is essential to define at least two lattice sites which have to be brought into overlap. All others are then readily determined due to the six-fold symmetry of the graphene lattice and by the constraint that a CNT has a cylindrical configuration. These two points can be connected by the so called chiral vector

$$\vec{C}_{n,m} = n\vec{a}_1 + m\vec{a}_2 \tag{1}$$

which is just a linear combination of $\vec{a}_1$ and $\vec{a}_2$ where n, m are integers and $m \geq n$. The imposed condition is due to the symmetry of the graphite lattice; the chiral vectors where $m > n$ have symmetric equivalents with $m < n$. Thus a given SWCNT can be characterized using a pair of integer indices (n,m), which together define the chiral vector of the nanotube.

This picture results from the two-dimensional graphene-sheet model, in which a CNT is described by a planar graphene sheet with periodic boundary conditions that take the translational symmetry along the circumference into consideration. This model provides the main features of the CNTs, although it suffers from a neglect of curvature effects.

The direction in which the graphene sheet has been wrapped, can be defined by the line along $\vec{C}_{n,m}$, to such an extent that the two points which are connected by $\vec{C}_{n,m}$, are overlapping. Thus, the circumference of the CNT is defined by through the following relation with the length of the chiral vector:

$$d_t = \frac{|\vec{C}_{n,m}|}{\pi} \tag{2}$$

where d_t is the tube diameter.

The six-fold symmetry of the graphene lattice provides a scheme for categorization of CNTs. All possible CNT structures can be classified by three general configurations of armchair CNTs, for which $n = m$, zigzag CNTs that have $n = 0$ and CNTs with all other chiralities. Often armchair and zig-zag nanotubes are also called chiral, despite the fact that their mirror images are identical to the original. Figure 2 shows a graphene sheet in which the real-space unit lattice vectors $\vec{a}_1$, $\vec{a}_2$ and the wrapping angle θ are depicted. The vectors of $\vec{a}_1$ and $\vec{a}_2$ have the same length of about 2.461Å.
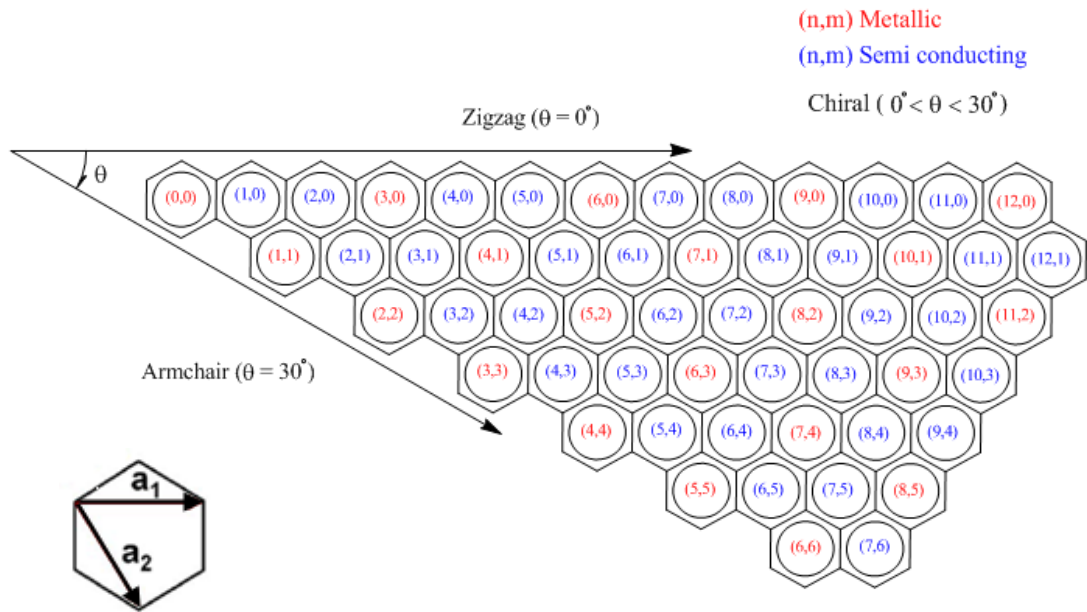
Figure 2 The sixfold-symmetry of the graphene sheet. The unit lattice vectors a_1, a_2, the chiral angle, (n,0) and (n,n)-lines are illustrated.[13]

By varying wrapping angles a variety of potential nanotube helicities can be achieved. These can be either left- or right-handed depending on the direction of rolling of the graphene sheet. The electronic system of CNTs displays strong 1D-character, as the absolute values of diameter and length (nm and μm, respectively) give rise to quantum size effects.[14]

Atomic structures of the two different CNT chiralities that are studied in this research work are shown in Figure 3 (*Software: Nanotube Modeler*).
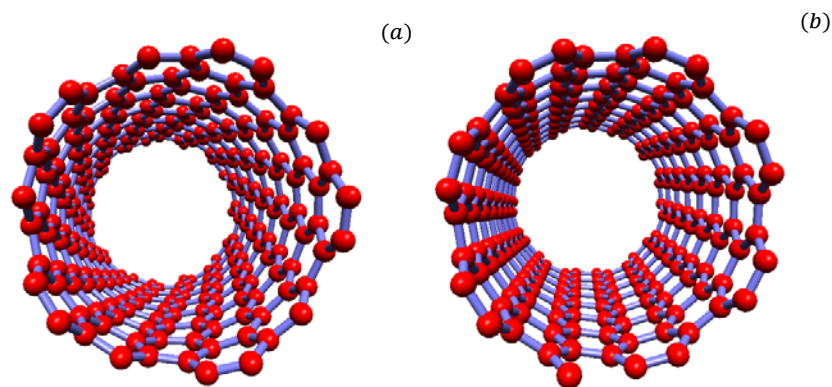
Figure 3 SWCNT atomic structure with (8,7) and (10,5) chiralities are shown in (a) and (b) respectively.

2.1.2 Synthesis of carbon nanotubes

Carbon nanotubes are manufactured by different methods in research laboratories and industry. The production of CNTs with a high order of purity, large amount, low costs, and uniformity remains one of the biggest challenges in the carbon nanotube community. The most commonly applied techniques are:

Chemical vapor deposition (CVD): In this technique, CNT is generated by decomposing hydrocarbon gases on a substrate in the presence of metal catalyst particles (Fe, Ni, Co). The synthesis of CNTs is often accelerated thermally or with plasma. MWNTs that are produced by this method mostly have high purity but with restricted control of the diameter and structure. CVD method can produce long nanotubes with diameters in the range of 0.6 - 4 nm for SWCNTs and 10 - 200 nm for MWNTs. The CVD technique is suitable for production of nanotubes at industrial scale. In plasma enhanced CVD, plasma is generated by the application of a strong electric field during the growth process. The growing nanotube will align with the direction of the electric field, adopting perpendicular orientation with respect to the substrate for instance. [15]

A high pressure (carbon monoxide) CO disproportionation or High pressure conversion of CO (HiPCO): This method is an improved version of CVD process in which carbon monoxide is used as a carbon source. HiPCO bases on the gas-phase growth of SWCNTs at high

temperature and pressure. This technique has proved successful in producing large quantities of SWCNTs with high purity. In this method, Fe $(CO)_5$ is inserted into a stream of CO gas at high pressure and temperature. The iron forms metal clusters that function as catalytic sites to help the Boudouard reaction: $2CO \rightleftarrows C(s) + CO2(g)$. It is widely held that when the metal clusters reach a size near that of C60 that they nucleate and grow to SWCNTs. This occurs because a SWCNT is a more stable form of carbon than a near spherical carbon overcoat of a metal cluster at diameters close to 1 nm. The metal and the SWCNT cluster grow in parallel until the metal cluster, attains a certain size that helps formation of a carbon shell around the cluster. This occurs by addition of residual free iron atoms. This sets an end to the growth of the SWCNT.[16]

Arc discharge method: This method is based on an electric arc discharge generated between two graphite electrodes under an inert gas atmosphere (argon, helium). A temperature higher than 5000˚C is required and a mixture of different components (including fullerenes, amorphous carbon, and some graphite sheets) is produced. The carbon nanotubes have to be separated from the soot and the catalytic metals present in the crude product. By choosing suitable control parameters (e.g. temperature, pressure, different gases and catalytic metals), it is possible to selectively grow SWCNTs or MWNTs. However length and diameter of the CNTs are poorly controlled. The resulting CNTs are often short with diameters ranging from 1.2 - 1.4 nm (SWCNTs) and 1 - 3 nm (MWNTs).[17]

Laser ablation: A graphite target is ablated and vaporized by the energy of laser irradiation. The ablation is carried out under flowing inert gas atmosphere at high temperature. Nanotubes produced in this way have high purity but the process is not appropriate for a large scale synthesis. In this way, bundles of individual SWCNTs of 5 - 10 μm in length and 1 - 2 nm in diameter are being made exclusively.[18]

Every one of these techniques is still under progress and subject to ongoing research. There are numerous variations of these methods designed for different conditions, with different set-ups, and corresponding process parameters. Every procedure provides diverse advantages and disadvantages over the quality and types of fabricated CNTs.

In this thesis, SWCNTs generated by two different synthesis techniques were used, namely Nanocyl SWCNTs and HiPCO SWCNTs:

Catalytic CVD (CCVD) is the method that produces Nanocyl SWCNTs. Nanotubes which leave the reactor are subsequently purified to above 70% carbon. This carbon nanotube has an average diameter of 2 nm.[19]

HiPCO process has been shown lately to produce nanotubes of high purity, with current purities of more than 90% atomic percent SWCNT carbon. The average diameter of HiPCO SWCNTs is roughly 1.1 nm. The dominant source of impurity in HiPCO nanotubes is the metal catalyst, which is encased in thin carbon shells and distributed all over the sample as 3-5 nm size particles.[20]

2.1.3 Mechanical, Electrical and Chemical properties of Carbon nanotubes

Amazing electro-mechanical properties of carbon nanotubes and their dimensions have made it the heart of various research areas. While a carbon nanotube has a diameter of the order of nanometer, its length can be more than 1 mm. Nanotube diameter is much less than nearly all advanced semiconductors devices available. Furthermore, the specific strength of SWCNT is predicted to be around 600 times more than steel.

Based on both experimental and theoretical researches, individual MWNTs have a tensile strength of 10 - 200 GPa and Young's modulus being over 1 TPa.[21] The elastic response of a nanotube to deformation is significant. CNTs investigations show that it can sustain up to 15 % tensile strain before fracture and the reversible bending of CNT is up to angles of 110º.[22]

Carbon nanotubes also have remarkable thermal and electrical properties. CNTs are thermally stable up to 2800°C in vacuum and up to 700°C under air which is about twice as high as diamond. Their thermal conductivity is about twice as high as diamond. They exhibit an exceptional electrical conductivity that enables them to carry electric current a thousand times better than copper wires.[22]

CNTs can be semi-metallic (often referred to as metallic), or semiconducting depending on their structure. CNTs can be used in organic based integrated circuits as conducting wires on a molecular scale, or possibly as an electrically active element. These as well as the usage of CNTs as almost a perfect model system for fundamental research, reflect the fascination of this molecular structure.[24]

Carbon nanotubes possess unique electrical properties. Its small diameter gives rise to quantum effects. The differences in the conducting properties of CNTs are attributable to the molecular structure. Depending on their chirality, CNTs can either be conducting or semiconducting. They are metallic if the integers of equation (2.1) are *n=m* and *n-m=3i* where *i* is an integer. All other structures are expected to be semiconducting[17] (Figure 2). The geometry of the nanotubes verifies band structures and hence the energy band gap. The energy band gap of semiconducting CNTs has an extreme dependency on the nanotube diameter and is given by [24]:

$$E_{gap} = \frac{2\gamma_0 a_{c-c}}{d} \tag{3}$$

Where γ_0 represents the C-C tight binding overlap energy (2.45 eV), a_{c-c} the nearest neighbor C-C distance (~1.42 Å), and *d* is the diameter of a nanotube. The inter-tube interaction of CNTs is strong and thus tubes are commonly observed in hexagonally packed bundles. This interaction for SWCNTs is quoted as ranging from 0.5 to 0.95 eV/nm. Various techniques are employed to debundle or isolate individual tubes, typically using surfactants or sonication. It is likely that inter-tube interaction is simply weak long-range covalent bonding, while it is often asserted to be of a van der Waals type. Interlayer interaction in graphite, often attributed to van

der Waals forces, can indeed be precisely modelled using density functional techniques which do not include any van der Waals type interactions.[25]

With such promising properties, CNTs are good candidates for reinforcement of advanced composites. Nonetheless, experimental data obtained from CNTs suffers from high variability and lab-to-lab inconsistencies remain to be resolved.

2.1.4   Functionalization and dispersion of carbon nanotubes

CNTs have poor solubility in most of the common solvents. To overcome this problem, carbon nanotubes are functionalized by physical or chemical attachment of certain molecules or functional groups to their surfaces. Functionalized CNTs are very attractive for physical and biological applications due to their strong sensitivity to chemical or environmental interactions. This leads to a wide range of applications, such as sensors. It is noteworthy that covalent and non-covalent functionalization, doping, decoration with organic as well as inorganic species of the surface of CNTs lead to direct changes of the optical, electrical, and mechanical properties of carbon nanotubes.

As mentioned previously CNTs in all their forms are difficult to dissolve and disperse in any aqueous and organic medium. Due to the strong attractive long-ranged van der Waals interaction, nanotubes have propensity to aggregate and form bundles or ropes, typically with highly entangled network structures (see section 2.1.3).

This attraction is fundamental for many body particle systems and well known for colloids dispersed in polymers. An attractive force between fillers also arises when suspended in a polymer. This is due to the entropic effects. Polymer chains in the region of the colloidal filler suffer an entropic penalty since nearly half of their configurations are prohibited. Therefore, there is a depletion of the polymer in this region. This causes an osmotic pressure forcing the filler particles to come together.

Homogenous dispersion of CNTs within a supporting medium is crucial for the fabrication of composites with improved properties, well defined and uniform structures. Intensive studies were therefore initiated on the exfoliation of carbon nanotubes in recent past. Broadly speaking, dispersion methods falls into two main categories: physical and chemical methods. The physical techniques involve physically separating the tubes from each other. The chemical methods frequently use surfactant or chemical modification of the tube surface. The drawback of the chemical methods is that certain types of aggressive chemical treatment can lead to the key nanotube properties being compromised.

In general, the functionalization of CNTs requires modifications of their surface chemistry supported by the mechanical agitation methods such as ultrasonication and shear mixing. Several functionalization strategies have been described recently. They are mostly based on the covalent and noncovalent coupling of surfactants and functionalities to CNTs.

Covalent functionalization methods refer to a treatment that involves bond breaking across the surface of the CNTs which disrupts the delocalized π-electron systems and fracture of σ-bonds and therefore leads to incorporation of other species across the CNTs' surface. Mechanical and electrical properties of the nanotubes change significantly if a defect is introduced to the CNT's. Covalent modification can be advantageous as it may improve the efficiency of the bonding between nanotubes and the host material (cross-linking). Therefore, improved mechanical performance can be achieved due to the enhanced interfacial stress transfer between the matrix and CNTs.

Non-covalent functionalization of the carbon nanotubes is highly desirable because no disruption of the sp^2 graphene structure occurs and the CNT properties are maintained. Its shortcoming concerns weak forces between wrapped (or coupled) molecules that may decrease the load transfer in the composite.

The chemical modification of the CNTs' surface increases solubility (or separation) of the nanotubes in a given solvent. An appropriate functionalization guarantees homogenous and stable dispersion throughout the solvent and in the composite host material. Furthermore, functionalities on the surface of CNTs may lead to enhanced interactions between filler and matrix, which is caused by the presence of the interfacial bonds between components. [26,27]

2.1.5 Applications of carbon nanotubes

Carbon nanotubes are suggested either as building-blocks or as active elements, in a large variety of nano-devices, ranging from (standard) field-effect transistors (FETs) [28], opto-electronic devices, bio-sensors[29] and nano-electromechanical systems (NEMS) [30]. The first electronic nano-device using CNTs to be built was the frequent FET with a back-gate. Interestingly, this principle design is still the starting point for majority of CNT-based nano-devices.

In the regular FET device design the CNT lies on top of predefined electrodes which themselves are positioned on the surface used as dielectric spacer (typically SiO_2 of a few 100 nm thickness) to the back-gate. In later versions of CNT-FET designs developed, the contact electrodes, source and drain, are identified on top of the CNTs because of contact stability. To raise the gate efficiency, approaches such as top-gates were developed. In this approach the gate was evaporated on top of the CNT. Another approach was aluminium back-gates, which take advantage of the natural aluminium oxide layer with a few nm thick as dielectric spacer.[31]

The bridge from a purely electronic CNT-device to a NEMS is trying to keep design as simple to build as possible. By selective etching, the tailoring of the dielectric spacer and the back-gate which lies beneath can be possible. In this way, several types of NEMSs, such as gigahertz-oscillators or prototypes of non-volatile memories have previously been constructed and studied.[31]

SWCNTs' unique size-related properties have led to commercial products such as strengthened, lightweight carbon composite sports equipment. Other impending applications include hydrogen storage media, nanoelectronic devices, sensors, field effect transistor, and energy storage devices. Application of carbon nanotubes as drug delivery carriers and diagnostic devices or as scaffolds for cell culture growth are exploring by biomedical researchers.[33]

SWCNTs have a variety of potential applications in material sciences and engineering because of their outstanding mechanical, electrical, optical, and thermal properties. There is however a technical problem that concerns the purity and homogeneity of SWCNT preparations. As described earlier, when SWCNTs are produced, they comprise bundles of nanotubes included of tubes with a distribution of lengths, chiralities, and diameters that are often contaminated with non SWCNT carbon. Further processing is needed before such mixtures are suitable for most applications and characterization methods. More specifically, methods are hence required to sort nanotubes by size and type and to get rid of the combinations of different nanotubes (bundles) and carbonaceous impurities. Reliable measurements of properties inherent to individual SWCNTs with low polydispersities can be made only after purification and sorting. SWCNTs have two primary forms of polydispersity, type (chirality and diameter) and length. In this thesis we will cover sorting of SWCNTs by type.

2.2 DNA

Biological molecules such as deoxyribonucleic acid (DNA) have shown great potential in fabrication and construction of nanostructures and devices. Double stranded DNA is the genetic material of most organisms and organelles, although phage and viral genomes may use single stranded DNA, single or double stranded RNA (ribonucleic acid). Most genetic information is encoded in the chemical language of DNA and reproduced in most cells of living organisms.[34]

2.2.1 Structure

DNA is a polymer made up from three components: nitrogen-containing bases, carbohydrate (deoxyribose) and phosphate. There are 4 types of nitrogen-containing bases in DNA. They are adenine (A), guanine (G), cytosine (C) and thymine (T). The sugar deoxyribose, forms, with phosphate groups, a very long backbone, alternating sugar-phosphate-sugar-phosphate, and so on. One of the 4 nitrogen containing bases is linked to every sugar molecule. Each unit of a phosphate, a sugar molecule and base is called a nucleotide and is about 0.34 nm long.

The double stranded helical structure of DNA is a key to its use in self assembly applications. Each helix or strand of the specific binding through 3 hydrogen bonds between cytosine and guanine and 2 such bonds between adenine and thymine can result in the joining of two complementary single stranded DNA to form a double stranded DNA. The joining of two complementary single strands of DNA through hydrogen bonding to form a double stranded DNA is called hybridization. If a double stranded DNA is heated above certain temperature, the two stands will start to dehybridize and eventually separate into single strands. As the temperature is reduced, the two strands will eventually come together and rehybridize to form the double stranded structure.

Each strand of the DNA is about 2 nm wide. A pitch is composed of 10–10.6 nucleotide pairs equivalent to 3.4–3.6 nm. Thus, constructions made from DNA will have nanoscale features. The phosphate groups are deprotonated in neutral pH and therefore DNA carries a negative charge, which results in electrostatic repulsion of the two strands. The charges are however neutralized by counter ions from the solution.[34]

In a DNA double helix, there exist groove like spacings between the strands. These voids are adjacent to the base pairs and are important functionally as they provide a binding site for target proteins. As the strands are not directly opposite each other, the grooves are unequally sized in ordinary B form DNA. One groove, the major groove, is 22 Å wide and the other, the minor groove, is 12 Å wide. Contrary to the minor groves, the width of the major groove makes the bases accessible. As a result, proteins like transcription factors that can bind to specific sequences in double-stranded DNA usually make contacts to the sides of the bases

exposed in the major groove. The geometry of the grooves change as DNA undergoes conformational transition from B form to other conformations.

Twisting double helical DNA leads to the formation of supercoil. When DNA is in its relaxed state, strand usually circles the axis of the double helix once every 10.4 base pairs. Upon twisting, the strands become more tightly or more loosely wound. If the DNA is twisted in the direction of the helix, this is positive supercoiling, and the bases are held more tightly together. If they are twisted in the opposite direction, this is negative supercoiling, and the bases come apart more easily. In nature, DNA often has slight negative supercoiling that is introduced by enzymes called topoisomerases. These enzymes are also needed to relieve the twisting stresses introduced into DNA strands during processes such as transcription and DNA replication.

DNA X-ray diffraction patterns suggest that the structure of DNA is a double-helix. However it is not a well-defined conformation but a family of related DNA conformations that occur at the high hydration levels present in living cells. Their corresponding X-ray diffraction and scattering patterns are characteristic of molecular paracrystals with a significant degree of disorder. [34]

DNA exists in many possible conformations that include A-DNA, B-DNA, and Z-DNA forms. In functional organisms however, only B and Z conformations are relevant. Different conformations differ in their handedness, depth and width of the grooves and their pitch size. In contrast to B-DNA, the A-DNA form is a right-handed spiral, with a shallow, wide minor groove and a narrower, deeper major groove. The A form appears under non-physiological conditions in partly dehydrated samples of DNA. However in vivo it is possible to be produced in hybrid pairings of DNA and RNA strands, as well as in enzyme-DNA complexes. The Z form occurs in segments of DNA that the bases are chemically modified by methylation. The strands roll up the helical axis in a left-handed spiral which is the opposite of the more regular B form. These atypical structures can be distinguished by specific Z-DNA binding proteins and may be involved in the regulation of transcription.[35]

Telomeres are specialized regions of DNA at the ends of the linear chromosomes. Since the enzymes that normally replicate DNA do not function in the extreme 3′ ends of chromosomes, enzyme telomerase does this task with the help of telomeres. In another words, the main role of telomers is to let the cell to replicate chromosome ends. In addition, telomeres protect the DNA ends and stop the DNA repair systems in the cell from treating them as damage to be corrected.

Telomeres can make the chromosome ends stable by forming structures of stacked sets of four-base units. Here, four guanine bases form a flat plate. These flat four-base units then stack on top of each other to form a stable G-quadruplex structure. Hydrogen bonds between the edges of the bases and chelation of a metal ion in the centre of each four-base unit stabilize the whole structure. There are also other structures that can be formed, with the central set of four bases. These bases may be either from a single strand folded around the bases or several different parallel strands, each putting in one base to the central structure.

Moreover, there are other telomeres formations that called telomere loops, or T-loops. In this large loop structures the single-stranded DNA curls around in a long circle stabilized by telomere-binding proteins. At the last part of the T-loop, the single-stranded telomere DNA is held onto a region of double-stranded DNA by the telomere strand disorderly the double-helical DNA and base pairing to one of the two strands. This triple-stranded structure is called a displacement loop or D-loop. Quadruplex structures can be used in nanotechnology to build geometric shapes. [34, 35]

2.2.2 Applications of DNA

Discovery of restriction enzymes and development of DNA purification and amplification methods in late twentieth century led to the emergence of DNA manipulation technology. Methods for manipulations of DNA have fundamentally changed the way questions are addressed in modern biology. DNA manipulation technology is often referred to as recombinant DNA technology. The techniques in recombinant DNA technology are intensively used in modern biology and biochemistry. Recombinant DNA is a synthetic DNA sequence that is an assembly from other DNA sequences. Their transformation into organisms can be done by using a viral vector, either in the form of plasmids or in the appropriate format. The genetically engineered organisms can be utilized to produce products such as recombinant proteins which can be used in medical research, or be grown in agriculture.

There are many different applications of DNA in can be seen in everyday life. For instance forensic scientists can use DNA at a crime scene to identify a matching DNA of a perpetrator. This technique is called genetic fingerprinting, or more accurately, DNA profiling. In this technique the lengths of variable sections of repetitive DNA, such as short tandem repeats, are compared between people. This method is usually a highly consistent technique for identifying a matching DNA.

Another application of DNA is in Bioinformatics which is a discipline that involves the manipulation, searching, and data mining of DNA sequence data. It provides techniques for mapping and analyzing DNA and protein sequences, aligning different DNA and protein sequences among others, aiming at increasing our understanding of biological processes.

On the other hand, developments in bioinformatics have led to widely applied advances in computer science, especially string searching algorithms, machine learning and database theory. String searching or matching algorithms can find an occurrence of a sequence of letters inside a larger sequence of letters and to search for specific sequences of nucleotides.

DNA contains historical information due to its mutations over time. Phylogeneticists can infer the evolutionary history of organisms, by comparing DNA sequences. Comparing DNA sequences within a species, the history of particular populations can be learned by population geneticists. This can be used in researches ranging from ecological genetics to anthropology. Besides, DNA has been used to observe modern family relationships.

DNA nanotechnology exploits the unique molecular recognition properties of DNA to create self-assembling branched DNA complexes with valuable properties. In this context DNA is seen as a structural material rather than as a carrier of biological information. Two milestones for DNA nanotechnology were the creation of two-dimensional periodic lattices (both tile-based and using the DNA origami method) as well as three-dimensional structures in the shapes of polyhedra. Nanomechanical devices and algorithmic self-assembly have also been realized, and these DNA structures have been used as templates to arrange and pattern other molecules such as gold nanoparticles and streptavidin proteins.[36]

Applications have been envisioned for DNA, in the assembly of devices and computational elements, for the assembly of interconnects or as the device element itself. The rationale for using DNA is that DNA is the molecule whose intermolecular interactions are the most readily programmed and reliably predicted where G pairs with C and A pairs with T. These properties make DNA a natural molecule of choice for programmed self-assembly. Second, DNA of any desired sequence can be readily produced by convenient solid support synthesis. Besides, DNA modifications with biotin groups and fluorescent labels introduced new applications for DNA in nanobiotechnology. Third, a toolkit of enzymes is available for manipulation of DNA molecules. Modifications can be made by a large group of enzymes that include restriction endonucleases, exonucleases, and DNA ligases.[37]

2.2.3 Functionalization of DNA

DNA molecules are used to functionalize various different structures for nanotechnological applications. Short double stranded DNA behaves like a rigid rod and can be used as rigid spacer at small scale structures. One interesting feature of DNA is that, branched DNA molecules can be designed. Such DNA branches occur in nature in replication and repair processes. The Holliday structure, a four-arm branched intermediate, is a well known conformation of DNA in recombination. This feature of DNA is very important in nanomaterial design[37] and finally DNA is used for functionalization of structures for its ability to self assemble and make specific and programmable interactions.[38]

DNA has been used as a basis for developing novel nano materials, making artificial networks, connecting molecules and nano scale objects to surfaces and assembling metal and semiconductor particles. For these applications, the target elements and molecules have to be functionalized with DNA. Different chemistries can be used for this aim. The choice of functionalization and immobilization methods depends on the application. For example, robust immobilization chemistries are generally preferred in order to avoid desorption of the probes from the sensing layer. Long term use, fast response, operational stability and reproducibility of the electrochemical biorecognition event, are some general aspects for employing the immobilization strategy.[39]

To functionalize surfaces with DNA, three methods are available: electrostatic binding, covalent binding, using antibody biotin/avidin linkage. The most widely used method is based on sulfur/gold chemistry. DNA molecule can be functionalized with a thiol or disulfide group. Thiol can in turn bind the gold. Since most of the nanoparticles carry charges, they can electrostatically adsorb biomolecules with different charges.

Switches that can be driven between two conformations are the simplest active DNA nanostructures. Their function is based on the changes in ionic conditions, temperature or by the binding of signaling molecule (often a DNA strand), which lead to an induced motion. [40]

Several strategies have been applied to synthesize Quantum dots and their arrays. Researchers were accomplished to assemble CdS nanoparticles using DNA as a template by making use of the electrostatic interaction between the phosphate groups in DNA double strands and the cationic surface modifiers on the CdS nanocrystals. On the other hand, other researches were done on this area by adopting a different approach by using DNA to assemble DNA fullerene hybrid organic materials. Their approach was to use, the negative phosphate backbone of DNA as a template to bind and organize C60 fullerene molecules modified with N,N-dimethylpyrrolidinium iodide moiety into defined mesoscopic architectures.[41]

The idea of DNA mediated self assembly has been broadened to metallic nanowires which have been operated as sensors. The principle of their function is the same as in a field effect transistor. In other words, it is based on the variations in chemical potential accompanying a target or analyte binding event (such as DNA hybridization), can act as field effect gate upon the nanowire and thus changing its conductance. [42]

A single crystal nanowire with a diameter between $10 \, \text{nm}$ and $20 \, \text{nm}$ is the perfect nanowire sensor. Here, a study on that was done on self assembly and subsequent mineralization of DNA in an electronic structure is demonstrated, as an example. In this study DNA was hybridized with complementary oligonucleotides attached to gold electrodes to create a single bridge spanning a gap of $12–16 \, \text{m}$.[43] Next was to produce a conducting nanowire. For that the DNA was used as a template for the directed synthesis of chains of silver nanoclusters from silver ions. The result from current voltage measurement shows that the conductivities are close to the bulk metal and it shows an ohmic behavior.

The first report of DNA functionalized CNTs and their effectively dispersion in water by sonication was published in 2002.[44] It turned out that short oligonucleotides having repeating sequences of guanines and thymines could wrap around a CNT. The wrapping was shown to have a helical manner with a periodic pitch. This discovery links one of the central molecules in biology to a technologically major nanomaterial, and opens the door to CNTs-based applications in biomedical technology.

The functionalization of CNTs with DNA molecules improves the CNT solubility in organic media dramatically. It can also be used to distinguish metallic CNT from semiconducting CNTs. DNA chains have a variety of functional structural groups available for covalent interaction with CNTs for building of DNA-based devices through the sequence-specific

pairing interactions. The best approach for DNA immobilization in CNTs is covalent binding on a solid surface by means of a single point attachment. The reactive sites on the CNTs were generated from the acid treatment to introduce the carboxyl groups on their tips. DNA molecules with functional linkers are then coupled to the carboxyl groups on the CNTs. SWCNT-DNA adducts can be obtained by carbodiimide assisted coupling of amine functionalized oligonucleotides to oxidized SWCNTs.[45]

Research investigations[5] indicate that DNA can absorb non-covalently as a single strand or double strand complex onto the surface of SWCNTS. For instance, DNA guided assembly of carbon nanotubes was done by using amine terminated DNA strands to functionalize the open ends and defect sites of single-walled carbon tubes. Furthermore, carbon nanotubes were found to be able to condense double stranded plasmid DNA to varying degrees which lead to the production of nanotube based gene delivery vectors. However the toxicity of carbon nanotube DNA hybrids should be examined in a similar approach to that of pure carbon nanotubes. In a relatively recent report, a piece of double stranded DNA wrapped around a single-walled carbon nanotube was used to detect optically DNA conformational polymorphism. The central part of the novel optical detection system was based on the transition of DNA secondary structure from the native, right handed "B" form to the alternate, left handed "Z" form which was modulated by metal ions. In proportion to this work, other reports[46] for the first time recorded that DNA destabilization and conformational transition induced by SWCNTS are sequence reliant. It is worth mentioning that all types of carbon nanotube DNA hybrids stated above have diverse electrostatic properties that depend on the diameter of the nanotube and electronic properties. These distinctions in properties allow the separation and chirality sorting of nanotubes with known separation thechniques.[47,48]

2.3 DNA-CNT hybrid formation

The proposal of utilizing DNA for CNT functionalization is not as exotic as it seems to be on the face of it. Two scientific investigation lines can be hinted as leading to this proposal. Studies on the interaction between the nitrogenous bases of DNA and different inorganic surfaces, such as graphite which is the most widespread, indicate that every one of the four nitrogenous bases of DNA have strong adsorption affinities to a graphite surface, although there are variations in the magnitude. Moreover, DNA bases can assemble on a graphite surface into a monolayer through hydrogen bonding interactions, in registration with the underlying lattice structure. There is a large molecular library of ssDNA exist. As a result of the structural diversities of ssDNAs that are based on the enormous number of sequences, there are definitely sequences in this library that can bind any given small molecule targets. The in vitro evolution method is a systematic way to find these sequences by the aid of molecular biology tools.[4]

The ssDNA library proposes interesting possibilities for CNT binding. The first idea was that depending on ssDNA's structure and sequence, aromatic bases in an ssDNA may be able to form π-stacking interactions with the side-wall of CNTs. However, there was no thought about the strength of these interactions.

The CNT binding sequences were searched based on the standard in vitro evolution procedure. It was during this process that strong DNA binding to CNTs was found and the idea of CNT dispersion by DNA was derived. In addition to ssDNA of almost any sequence, short double-stranded DNA, and total RNA extracted from bacteria can also disperse CNTs, as schematically shown in Figure 4.
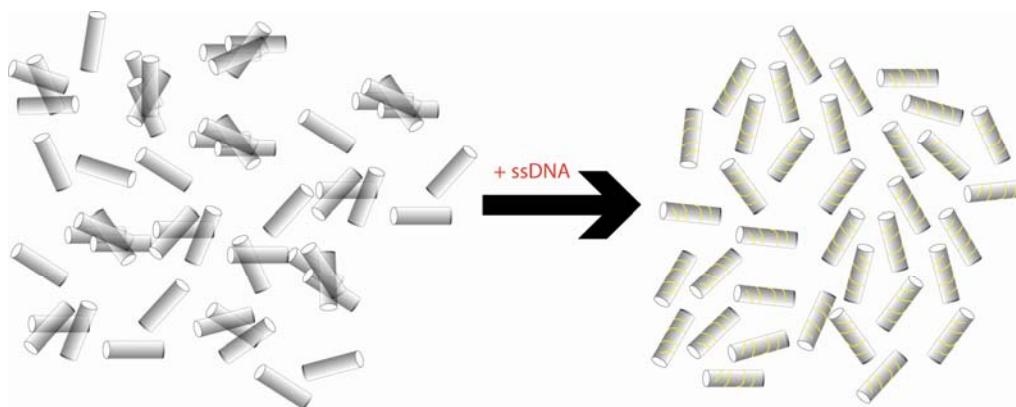
Figure 4 Schematic view of SWCNT dispersion via ssDNA functionalization.

A basic molecular dynamics simulation, that did not include solvent, suggested a helical structure for the structure of ssDNA on a CNT. In this simulation the bases are stacked onto the CNT surface and the sugar-phosphate backbone is extended outward. Later, measurements were done by CD spectroscopy on DNA-CNTs and also confirmed the helical wrapping structure. In the molecular dynamics simulations that were recently done the effect of aqueous solvents is included. It was demonstrated that ssDNA has a high tendency to form a helical wrapping from the 3' end to the 5' end which is due to the electrostatic and torsional interactions within the sugar-phosphate backbone.

For the helical wrapping, there is an optimal pitch for CNT and a specified sequence. The helical pitch strongly influences the electrostatic field near it. This is attributable to the direct relation between the helical pitch and the linear charge density of the hybrid. Therefore helical pitch of ssDNA-CNT hybrid is a key parameter controlling separation in IEX.[50-52]

2.3.1 DNA-CNT hybrid energy estimation

DNA-CNT assembly is potentially based on the contribution of some physical effects, such as entropy loss caused by the confinement of the DNA backbone, electrostatic interactions between DNA charges, van der Waals and hydrophobic interactions between DNA bases and the CNT, and CNT deformation. Calculations for finding the binding energies of DNA to CNT resulted in a strong binding energy of about 10 kT per nucleotide. That is while there are trivial variations among the four nucleotides. These differences are mainly due to the π-π stacking interaction, other than the involvements of the sugar-phosphate backbone.

Adhesion between DNA bases and the carbon nanotube is the main driving force of DNA-CNT hybrid formation. Adhesion comes from the interaction between the base and the CNT due to van der Waals and hydrophobic interactions which is favorable. Although trustworthy values for CNT−base interactions are not available, researchers have looked at the binding of nucleic acid bases to graphite, explaining that the binding energy drops off with a value of about 8 k_BT per base, which is at room temperature ($T = 300$ K). The series of the binding energy reduction is G > A > T > C. If we take a very simplistic approach and we assume that the interaction of oligonucleotide with SWCNT can be reduced to the sum of interactions of individual bases[53] with the tube then the following binding energies will be estimated for $(TTTA)_3T$ and $(CCG)_2CC$ sequences:

Table 2-1 ssDNA-CNT binding free energy F_{bind}, F_{vdw} and F_{res} are the electrostatic, van der Waals, and position-restraint contributions to F_{bind}, respectively. All values are in kcal.mol^{-1}.

Oligonucleotides	ΔF_{ele}	ΔF_{vdw}	ΔF_{res}	ΔF_{bind}
$(TTTA)_3T$	-1.9 ± 0.36	-106.8 ± 1.08	5.5 ± 0.36	-102 ± 1.37
$(CCG)_2CC$	-0.6 ± 0.28	-60.2 ± 0.812	3.8 ± 0.28	-60.8 ± 1.13

The adhesion energy is significantly larger than k_BT per persistence length which is due to the interval between neighboring phosphorus atoms on the DNA backbone is 6−7 Å, as the persistence length for ssDNA is 1.6 nm at a 150 mM salt concentration. There are two primary differences between the bases. First is because of the different sizes of purines and pyrimidines and the second one is the variations in hydrophobicity. In addition, it is known that interbase hydrogen bonding has the role of stabilizing ordered monolayers formed from bases, in numerous cases. Therefore, it is believed that hydrogen bonding has an important effect on the binding energy. It is interesting to know that the efficiency of homopolymeric ssDNA as a dispersant for CNTs pursue a different sequential manner which is T > C > A, (because of poly-dG's insolubility in water, guanine is inaccessible experimentally). It is north worthy to mention that the difference between the behavior of single bases and of homopolymers is partially due to the difference in the number stacked and unstacked bases.[54]

Another parameter that has a role in DNA-CNT formation is the decrease of entropy due to confinement of DNA backbone. In order to find the order of magnitude of entropic loss due to confinement of backbone degrees of freedom, one may think about the required free energy(F_c) to stretch the ends of a freely jointed chain with persistence length b_k and number of segments N to a distance R.

$$\boldsymbol{F}_c = \frac{2}{3}k_BT\frac{R^2}{Nb_k^2} \qquad (4)$$

The above equation is accurate merely for a small stretches compared to Nb_k, and it makes it possible to achieve estimation (with an order of magnitude) of the entropic free energy by replacing R by Nb_k

$$\boldsymbol{F}_c = \frac{3}{2}Nk_BT \qquad (5)$$

that is, about k_BT per Kuhn length. As it was mentioned in earlier the persistence length of ssDNA is approximately 1.6 nm at the monovalent salt concentration of 150 mM. Frequently, in these studies the ionic strength is significantly smaller, and in these situations, the persistence length can be considerably larger. Consequently, in contrast to the adhesion energy, the free energy increase as the result of entropy loss caused by the minute confinement of the backbone. Experimental measurements also confirm this conclusion. These measurements prove that ssDNA necessitates no more than about 5 pN under 150 mM salt concentration to be stretched halfway to full length. This entropy loss is estimated to vary in the range of 0.4−1.3 k_BT per nm of the nanotube for a wrapping angle of 45° and Kuhn lengths in the range of 16−50 Å.

At small ionic strength, in particular, electrostatic interactions among ions, the backbone charges, and also between them and the nanotube play a significant role in DNA-CNT formation and stability. The electrostatic energy of interaction, F_{el}, can be calculated using Manning's counterion condensation theory for a line of charges

$$\boldsymbol{F}_{el} = \left[-\frac{1}{z}\left(2 - \frac{1}{z\xi}\right)\log(1 - \exp(-kb)) - \frac{1}{z} + \frac{1}{z^2\xi} \right] ;$$

$$\xi = \frac{l_{\mathrm{B}}}{b} = \frac{q^2}{(4\pi\varepsilon\varepsilon_0 k_{\mathrm{B}}Tb)}$$

(6)

where z is the valence of the counterions and ξ is the ratio of the Bjerrum length l_{B} to the distance between adjacent charges along the line, b. ε_0 and ε are the dielectric constant of permittivity of free space and water, respectively, q is the magnitude of the charge of an electron, and κ is the reciprocal of the Debye screening length. For 100 μM monovalent salt at room temperature and for a range of wrapping angles ($0-3\pi/8$), F_{el} is in the range of $1.8-3.8$ $k_{\mathrm{B}}T$ per nm. In conclusion, the less the ionic strength, the more dominate the electrostatic contribution over entropic terms.[55, 56]

It is very improbable that extensional stiffness of DNA plays a significant role in the free energy. One reason is that this stiffness plays a role only at stretches close to the contour length. Another reason is the lack of restraints on the backbone length of ssDNA on a CNT. However the enthalpy of bending and torsion of the DNA backbone should be considered. Numerous studies of wrapping polymers around cylindrical objects, assign bending and torsion energy. If we consider ssDNA as an object with a persistence length of 1.6 nm or larger, we may expect elastic bending energies to be a key in wrapping it around a cylinder with a diameter on the order of 1 nm. However, there may not be significant enthalpy of bending and torsion, if the value of the persistence length is mostly because of electrostatic stretching and the underlying null ssDNA is much more flexible. Evidences in molecular simulations enlighten that the latter is the case. Therefore the intrinsic bending and torsional stiffness of ssDNA are neglectable by directly accounting for electrostatic effects.

When CNTs diameter is more than a critical diameter, the ability of CNT's sidewalls to deform, strongly influences the adhesion between them. The deformation is in a way that the area of contact is further increased. The critical diameter is about 10 Å and therefore, for larger diameter CNTs, it is probable that DNA adhesion will cause considerable deformation.[54, 57]

2.4 Discussion on Methods

As described in the background, CNT separation problem has received significant attention over the last few years. In particular DNA-CNT hybrids have been used for structure-based sorting of CNTs. DNA-CNT hybrid carries a net negative charge due to deprotonation of backbone phosphates. The magnitude of negative charge density on the CNT is a function of the DNA sequence and the electronic properties of the tube. Such differences can be exploited to solve CNT separation problem. For this aim, ion–exchange liquid chromatography (IEX) is the method of choice which is widely used in chemical and biochemical labs, and in the pharmaceutical industry. The main ingredient of this technique is adsorption and desorption of the target molecules on charged surfaces in a controlled manner. The output of IEX is monitored by optical absorption spectral changes from fraction to fraction. The outcome of separation process is known to have strong dependence on the DNA sequence.[4, 49]

The result of the separation process needs to be characterized accurately. There exit handful of different analytical tools that are proved suitable for characterization of the degree of functionalization of carbon nanotubes, including conventional microscopy techniques such as transmission electron microscopy (TEM), scanning electron microscopy (SEM), scanning tunneling microscopy (STM), and atomic force microscopy (AFM), as well as spectroscopic techniques such as Raman spectroscopy and UV–visible–near IR spectroscopy. Characterization of functionalized carbon nanotubes is a field under development. A number of major challenges have remained to be resolved. One such challenge is the inconsistencies between the AFM and STM investigations of the extent of nanotube functionalization reported in the literature. [49, 51]

Conventionally, Raman spectroscopy was the method of choice for probing the extent of covalent sidewall functionalization. Covalent binding of addends leads to characteristic changes in the intensity ratios of SWCNT Raman bands. The most evident change is a raise in the intensity of the D band, which arises from the generation of sp^3 hybridization of carbon atoms as defects in the sidewalls.

A good measure of the extent of functionalization is therefore the intensity ratio between the D band and the G band. However, lately it has been reported that in addition to the interpretative issue of an asymmetric Fano line shape of the G band peak, metallic tubes often exhibit considerable D-band intensities even within the same sample and that this complicating difference between metallic and semiconducting tubes arises from a double resonance process. One other factor that affects Raman signals is aggregation of functionalized CNTs.[58]

The complementarity of other techniques is very informative. Luminescence spectroscopy and microscopy have become practical techniques for probing the dispersion of functionalized nanotubes in polymeric nano-composites where collection of Raman data has not been straightforward.

Optical studies show that the electronic density of states of SWCNTs possesses spike-like features known as van Hove singularities. Optically permitted transitions between van Hove singularities can typically be observed in the UV–visible–near IR region.[49, 59]

In this current study the preparation of hybrids of ssDNA with SWCNTs and IEX chirality-separation of SWCNTs is reported. Atomic force microscopy (AFM) and UV-vis absorption spectroscopy were performed in order to characterize the resulting hybrids.

2.4.1   Ion Exchange Chromatography

Chromatography is an umbrella term for a range of physico-chemical separation techniques, all of which have in common the distribution of a component between a mobile phase and a stationary phase. The various chromatographic techniques are subdivided based on the physical state of these two phases.

Two major chromatographic techniques in chemical analysis are Gas Chromatography (GC) and High Pressure Liquid Chromatography (HPLC). The technique of HPLC flourished after it became possible to produce columns with packing materials made of tiny beads (10 μm) and to operate them under high pressure.

Ion-Exchange Chromatography (IEX) separation method is based on ion-exchange processes taking place between the mobile phase and ion-exchange groups bonded to the support material. In highly polarizable ions, an additional contribution to the separation mechanism comes from non-ionic adsorption processes. The stationary phase is composed of polystyrene, ethylvinylbenzene, or methacrylate resins co-polymerized with divinylbenzene and functionalized with ion-exchange groups. Ion-exchange chromatography is utilized for the separation of both inorganic and organic anions and cations.

2.4.1.1   Theory of Ion Exchange Chromatography

Separation in ion exchange chromatography relies on the reversible adsorption of charged solute molecules to immobilized ion exchange groups of opposite charge. Ion exchange experiments are often performed in three central stages.

The first stage is equilibration in which the ion exchanger is brought to a starting state, in terms of pH and ionic strength, which allows the binding of the desired solute molecules. At this stage the exchanger groups are associated with exchangeable counter-ions (typically simple anions or cations, such as chloride or sodium).

In the second stage, the sample is introduced and adsorption takes place. Solute molecules carrying the appropriate charge displace counter-ions and bind reversibly to the column. Unbound substances can be washed away from the exchanger bed using starting buffer.

In the third stage, substances are removed from the column by reducing the affinity of the solute molecules to the column. That is done by changing to elution conditions unfavorable for ionic bonding of the solute molecules. This usually involves increasing the ionic strength of the eluting buffer or changing its pH. In this studies desorption is achieved by the introduction of an increasing salt concentration gradient, resulting in releasing the solute molecules from the column in the order of their strengths of binding. In other words, bound substances are eluted in the reverse order of their bonding strength, the most weakly bound substances being eluted first.

2.4.1.2 The matrix and charged groups

An ion exchanger consists of an insoluble matrix to which charged groups have been covalently bound. The charged groups are neutralized by associated mobile counterions. These counter-ions can be reversibly exchanged with other ions of the same charge leaving the matrix unaltered.

Exchangers may carry positive or negative electric charges. Positively charged exchangers have negatively charged counter-ions (anions) available for exchange and are called anion exchangers. Conversely, negatively charged exchangers have positively charged counter-ions (cations) and are termed cation exchangers. Various matrices are available in terms of chemical compositions; they may be based on inorganic compounds, synthetic resins or polysaccharides.

The physico-chemical nature of the matrix defines its chromatographic properties such as efficiency, capacity and recovery as well as its chemical stability, mechanical strength and flow properties. The nature of the matrix will also influence its behavior towards biological substances in terms of biocompatibility and the preservation of biological activity.

The existence of charged groups is a key property of an ion exchanger. The type of functional group defines the type and strength of the ion exchanger; their total number and availability determines the capacity. For example, Sulphonic and quaternary amino groups are used to form strong ion exchangers; other groups form weak ion exchangers. It must be noted that the strength of binding is not necessarily strong in a strong ion exchanger. The terms strong and weak refer to the degree of variation of ionization as a function of pH and not the binding strength. Strong ion exchangers are in their fully ionized state over a wide pH range whereas with weak ion exchangers, the degree of dissociation and thus exchange capacity show much stronger pH dependence.

In strong ion exchangers the following properties can be observed:

• Due to loss of charge from the ion exchanger the sample loading capacity does not decrease at high or low pH values.
• Interactions between the ion exchanger and the solute are mechanistically very simple.
• Since the charge characteristics of the media do not change with changes in pH, ion exchange experiments are more controllable.[60]

2.4.1.3 The Ion Chromatographic System

The basic components of an ion chromatograph are shown schematically in Figure 5. It is similar to the conventional HPLC setup.
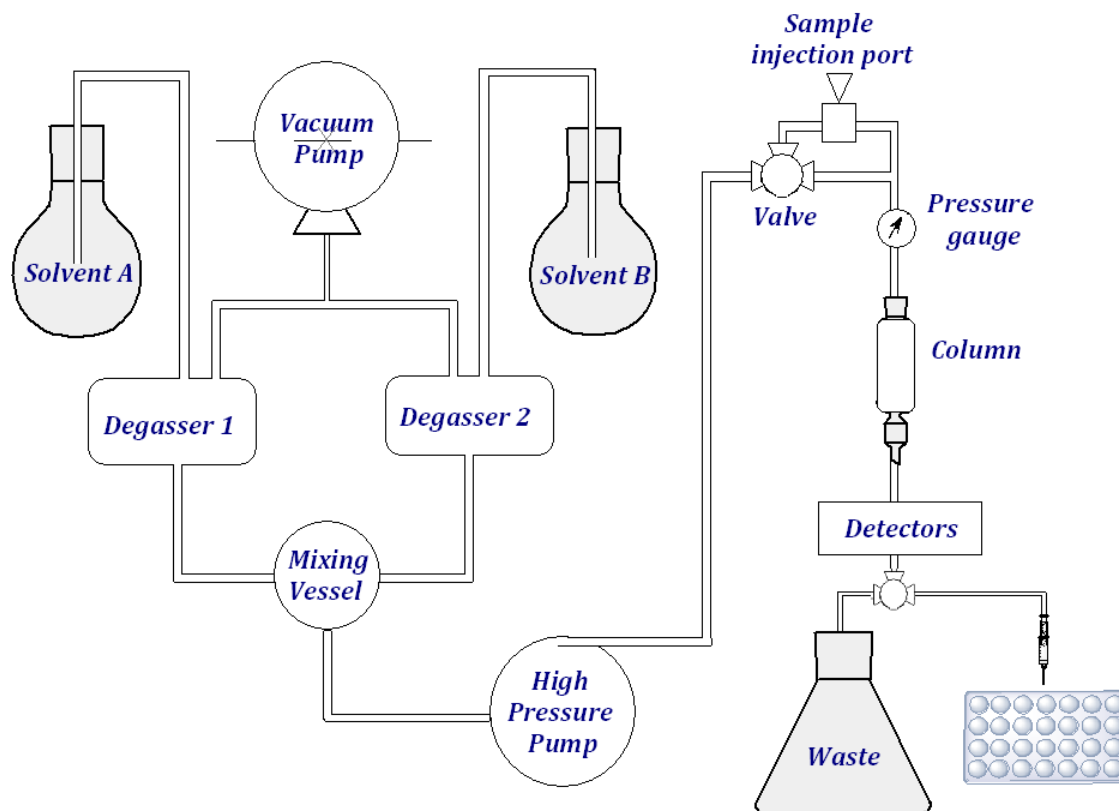
Figure 5 Basic components of an ion chromatograph.

The mobile phase is pumped through the chromatographic system. Normally, either single-piston or dual-piston pumps are used. The flow of eluent is required to be pulse-free in order to have sensitive UV-Vis and amperometric detectors.

To achieve this, pulse dampers are employed with single-piston pumps and a sophisticated electronic circuitry with dual-piston pumps. The sample injection is done via a loop injector. The system is equipped with a three-way, with two ports being connected to the sample loop. The sample loading is performed out at atmospheric pressure. After switching the injection valve, the sample transportation is done to the separator column by the mobile phase.

The separator column is the heart of the chromatographic system. The quality of the analysis depends on the choice of a suitable stationary phase and the chromatographic conditions. The

column tubes are fabricated from inert material such as Tefzec, epoxy resins, or PEEK (polyether ether ketone). Normally, the system is operated at room temperature.

Only in exceptional cases - for example for the analysis of long-chain fatty acids – separation is carried out at elevated temperature to ensure analyte solubility. In order to improve peak efficiencies, an elevated column temperature is also recommended for the analysis of polyamines.

The analytes are detected and quantified by a detection system. Like any detection system, the performance of the detector is evaluated based on sensitivity, linearity, resolution (detector cell volume) and noise (detection limit).

In ion chromatography, detection is often based on conductivity measurement. Conductivity detectors are used with or without a suppressor system. The main role of the suppressor system as part of the detection unit is to convert the sample ions into a more conductive form, and to chemically reduce the high background conductivity of the electrolytes in the eluant. In addition to conductivity detectors, UV-Vis, amperometric, and fluorescence detectors are in use for this aim.

The chromatographic signals can be displayed on a recorder in real time. Ion chromatography is a quantitative technique. Quantification is done by evaluating peak areas or peak heights, both of which are proportional to the analyte concentration over a wide range. Traditionally this was performed using digital integrators which are connected directly to the analog signal output of the detector. Nowadays digital integrators are no longer in use, due to low computer prices and lack of GLP/ GLAP conformity. Modern detectors possess an additional parallel interface that enables the connection to a personal computer with suitable chromatography software installation that allows a fully automated operation of the chromatographic system.

Because corrosive eluants such as diluted acids and bases are often used in ion chromatography, measures have to be taken to prevent corrosion of the components. In conventional HPLC systems stainless steel was used for fabricating the tubings and pump heads. Consequently such systems are only partially suited for ion chromatography, because even stainless steel is corroded in the long run by aggressive eluants. Moreover significant contamination problems would result, because metal ions exhibit a high affinity towards the stationary phase of ion exchangers, leading to a significant loss of separation efficiency. Additionally, metal parts in the chromatographic fluid path would make the analysis of orthophosphate, complexing agents, and transition metals more complicated and tricky. Thus all parts of the chromatographic system being exposed to these liquids should be made of inert, metal-free materials.[60]

2.4.1.4 Chromatographic separation of DNA-CNT hybrids

According to section 2.3, the negative charge of the DNA-CNT hybrid is from deprotonated phosphates of the DNA backbone. These interactions and those between eluting salt solution and the resin are electrostatic in nature, and depend on the linear charge density of the hybrid.

There are two contributions to the net charge, one being the linear charge density of the phosphate groups along the nanotube axis. This is then modulated by differences in the electronic character of the nanotube core.[5]

In the case of metallic tubes, electrostatic field associated with the charged DNA, induces positive screening image charges in the nanotube. These results in a reduction of the net linear charge density of the DNA-CNT hybrid, from that of the DNA wrap alone. In semiconducting tubes, an increased effective linear charge density of the DNA-CNT hybrid relative to that of the DNA wrap alone is observed. That can be explained by considering the fact that polarizability of the nanotube is lower than the polarizability of the surrounding water. By applying an image charge analysis for adjacent dielectrics, an increase in the effective charge density can be explained.[54]
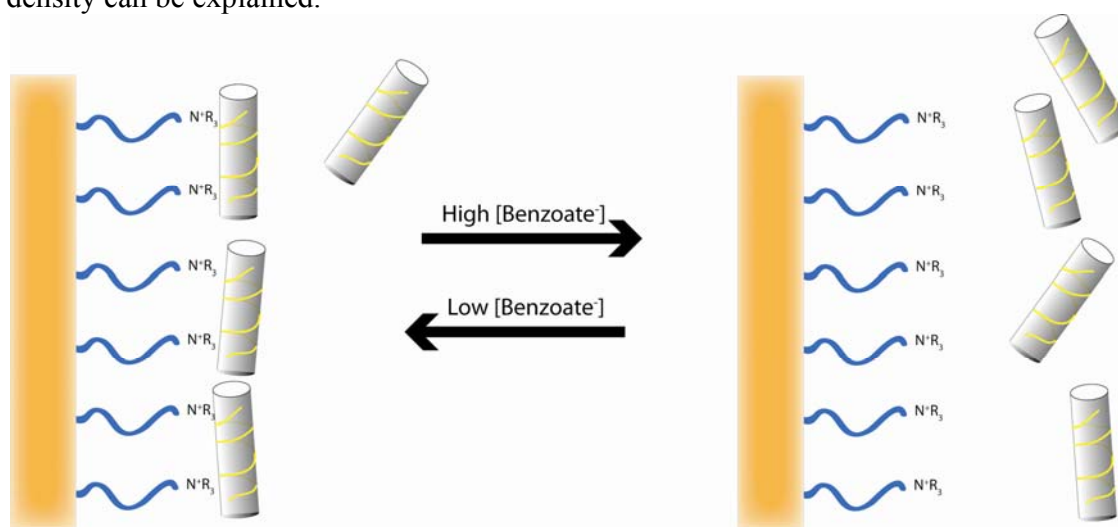
Figure 6 Mechanism of separation of DNA-CNT in IEX process.

As a consequence of this fundamental difference in behavior, a remarkable contrast can be seen in the binding strengths of metallic and semiconducting nanotubes to the anion exchange resin. There are two non-exclusive mechanisms for semiconducting DNA-CNTs that are responsible for the dependence of linear charge density on tube diameter. First, the linear charge density of the DNA varies with tube diameter due to wrapping geometry changes. Second, since the polarizability of semiconducting nanotubes depends on diameter, the effective linear charge density is diameter-dependent. Consequently the diameter-dependent separation of semiconducting tubes, are allowed.[51]

Previous studies revealed the sequence specificity of oligo-SWCNT interaction. The binding of ssDNA to SWCNT happens via motifs of 8-14 nucleotide length. In terms of sequence, alternating appearance of purines and pyrimidines such as …. PuPyPuPy… was reported. Long ssDNA with such motifs wrap around SWCNT in an ordered fashion. This has been observed in MD simulations and confirmed by experimental observation of the conformation

of the hybrid. For short sequences, an ordered binding of the DNA molecules to the tubes is not very likely.

For having an efficient IEX separation, we need to have an ordered coverage of the tubes with the DNA molecules. This is because an ordered DNA structure tiles the SWNT side-wall and minimizes its van der Waals and hydrophobic interactions with the IEX resin. This leads to early elution of the hybrid and the peak will be narrow as well. Therefore hybrids with long DNA strands are more suitable for such analytical separations. If there would be a way to make ordered DNA coverage with short sequences, such hybrids would be suitable for IEX separation. How can we achieve this goal?

Using MD simulation, and by being inspired by ordered 2D adsorption of short DNAs to graphene sheet, it has been shown that only particular short DNA sequences satisfy the geometric requirements for forming ordered assembly on the tube surface. One such sequence is $(ATTT)_3$. This can be explained in details if we know all the physical interactions. But a qualitative picture can be achieved based on thermodynamic analysis.

In a qualitative approach, the degree of order of adsorbed DNA can be described by an order parameter p. The free energy functional can be written as a function of DNA sequence, nanotube structural parameters and the order parameter of the hybrid: *G = G (sequence, (n,m), p)*. By minimizing this function, order parameter will be estimated for equilibrium state.[51]

In summary, p determines separation quality by IEX. For a random short sequence p is small for all (n,m). For short sequences with alternating Pu and Py, p is large for one or few (n,m) and is small otherwise. This is the basis for the protocol used in this thesis. This protocol works for semiconducting tubes better than metallic ones as the former has a weak free energy dependence on n and m.

The mechanism of molecular recognition in this process is geometric in nature in contrast to the more commonly seen energetic mechanism.

2.4.2   Optical Spectroscopy

Different molecules absorb radiation of different wavelengths depending on the structural groups of the molecules. Absorption of incident radiation by bonding or non-bonding electrons correspond to a high energy transition (~100 kCal/ mole). That appears as an absorption band in the high frequency (low wavelength) region of the spectrum at 200 - 800 nm in the UV and visible range of detection. Presence of solvent leads to broadening of the bands and a dramatic loss of resolution. In contrast, vibration fine structures can be resolved in gas phase. Similarly sharp peaks appear within a continuum in non-polar solvents.

Figure 7 presents a beam of monochromatic radiation of radiant power I_0, directed at a sample solution. Absorption takes place while the beam passes the sample and the outgoing beam has radiant power I ($<I_0$).

Figure 7 Schematic view of a sample illuminated with a monochromatic laser beam.
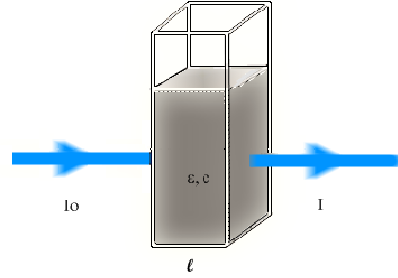
For a solution of an absorbing substance, transmittance at a monochromatic wavelength is defined as

$$T = I / I_0 \tag{7}$$

In the case of homogenous non-scattering sample, transmittance is logarithmically related to concentration and optical path-length:

$$\text{Absorbance (A)} = \log_{10} (I_0 / I) = \kappa.c.l \ /2.303$$
$$\varepsilon = \kappa/2.303 \tag{8}$$

where c (*mg/ml*) is the concentration of solute and l (*cm*) is the distance travelled between parallel optical faces of a suitable cell, k is a proportionality constant and ε is called molar absorptivity coefficient. Equation 8 is known as is the Beer Lambert law. [61]

2.4.2.1 Optical absorption spectroscopy of DNA-SWCNT

The optical characteristics of single walled carbon nanotubes reflect their unusual electronic structures. The optical absorption spectra of SWCNT in the UV–Vis–NIR range drive from electronic transitions within one dimensional joint density of states (JDOS) of the tubes. The JDOS function is defined by

$$JDOS(E) = \sum_J \int \frac{\Gamma dk}{2\pi[E - 2E^C(J,k)]^2 + \Gamma^2} \tag{9}$$

where the summation index J is the angular momentum quantum number corresponding to the different sub-bands, Γ a phenomenological level broadening parameter, and E^C the conduction band dispersion. [62]

A typical feature of one-dimensional crystals is that their DOS is not a continuous function of energy, but it slides down gradually and then rise in a discontinuous spike. On the contrary, three-dimensional materials have continuous DOS. In one-dimensional materials these sharp peaks are called Van Hove singularities. Therefore in optical experiments one observes not a continuous absorption spectrum above the absorption edge, but rather a set of separate peaks,

corresponding to transitions between different Van Hove singularities. There are certain selection rules related with these transitions. In particular in metallic tubes one cannot observe the transitions between the closest conduction and valence bands. The DOS of such metallic band is non-singular, while the overlaps of these bands at the Fermi point made the enhancement of non-radiative recombination mechanism possible.

Each Van Hove singularity is labeled with the index of the sub band to which it belongs. Optical absorption spectra of SWCNT ensembles display three broad bands in the UV–vis–NIR region. Of the three major features at ~0.9, ~1.5 and ~2.0 eV, the first two correspond to clusters of E_{11}^S and E_{22}^S transitions in semiconducting SWCNTs, respectively, while the third peak relates to clusters of E_{11}^M transitions in metallic tubes.

A theoretical graph which is called Kataura plot relates SWCNT indexes (n,m) and its band gap energies. Since the transitions are relatively sharp, having the UV-vis-near IR spectrum of a CNT one can figure out its chirality.[63-65, 13]

2.4.3 Atomic Force Microscopy

The Atomic Force Microscope (AFM) is a well-established method of imaging nanoscale structures. In contrast to vacuum techniques like Transmission Electron Microscope (TEM) and the Scanning Electron Microscope (SEM), an AFM is not restricted to imaging in a vacuum environment and the sample preparation is far easier with an AFM than with a TEM.

Furthermore there is a growing interest in the usage of AFM in nano-manipulation and nano-assembly. AFM is playing a highly promising role in the field of molecular biology too.

The working principle of an AFM is to characterize a sample by bringing a sharp probe in close proximity to the sample surface. The probe tip senses the surface forces that can be either attractive or repulsive. As a result of the forces, the cantilever on which the tip resides undergoes a deflection which is detected in real time. Deflection can be monitored either by tunneling detection, or optically. The latter is the method of choice currently. In this method which is called optical lever, a laser beam is bounced off of the cantilever and back onto a split photo detector. A typical AFM photo detector has four quadrants, allowing both the longitudinal bending modes and lateral torsional modes of the cantilever to be monitored. The deflection in the cantilever results in a push pull signal on the detector which can be used to construct a feedback loop in order to control the tip-sample interaction force.

Interestingly imaging depends entirely on a feedback control loop. Most AFMs use piezo-electric actuators, optical detection of cantilever deflection, and a proportional–integral–derivative (PID) controller. AFMs can operate in a variety of modes, including contact mode and dynamic mode.

In contact mode, the tip is moved across the surface while the feedback loop minimizes the deflection of the cantilever with reference to its nominal position. This mode is also known as constant force mode because controlling the deflection of the cantilever is equivalent to having the surface interaction force under control. One of the applications of this mode is imaging of the materials that are not damaged by being in sheer with a sharp tip.

One of the advantages of contact mode is that scanning with a high speed and images with atomic resolution is possible to be obtained. In addition scanning of rough samples with extreme changes in vertical topography is easier in this mode. However Lateral forces in contact mode can distort the image and capillary forces from a fluid layer can cause large forces normal to the tip-sample interaction. Combination of these forces reduces spatial resolution and can cause damage to soft samples.

The force measured by AFM can be classified into short range forces and long range forces. When we scan at large distances from the surface, the long range forces dominate. These forces can be generated from van der Waals force, capillary forces (due to the water layer often present in an ambient environment). The short range forces are very important when the scanning is in contact with the surface, in particular the Pauli Exclusion Principle forces.

In dynamic mode AFM the cantilever is oscillating in the proximity of the surface at a frequency close to the resonant frequency of the cantilever. The oscillation amplitude and consequently the tip-sample interaction remains constant by an electronic feedback loop. In this mode, the amplitude of the oscillation is slightly less than the nominal tip-surface distance.

The most common form of dynamic mode is so called AC mode, intermittent contact mode or tapping mode. In this mode the amplitude of the free oscillation is slightly larger than the nominal tip-surface distance. When the tip comes into close to the surface, the oscillation frequency, amplitude and phase are modulated. Detection of this modulation and closing a feedback loop on the amplitude of the oscillation, this amplitude can be maintained at a constant level. Once again, the control signal represents the surface topography.

The advantages of the tapping mode are the removal of a large part of permanent shearing forces and causing less damage to the sample surface, even with more rigid probes. Various components of the sample exhibit different adhesive and mechanical properties and therefore show a phase contrast. This allows a compositional analysis. For a good phase contrast, larger tip forces are of advantage, while minimization of this force lessens the contact area and facilitates high-resolution imaging. Hence in applications it is necessary to choose the right values matching the objectives. The primarily used probe for tapping mode applications are Silicon probes.

Forces that act between the sample and the tip result in the variations in the resonant frequency, phase and oscillation amplitude of the cantilever. The amplitude is used for the feedback and the vertical adjustments of the piezo scanner are recorded as a height image. At the same time, the phase and amplitude changes are presented in the phase and amplitude image respectively.

The alteration in the length of the z-axis on the xyz-scanning piezo tube makes is possible to monitor the vertical position of the probe tip. The length of the tube is proportional to input voltage to the scanning piezo tube. The change in the z-axis is plotted as a topographical map of the sample surface. Although it is possible to measure of the height of surface features with this data, it does not indicate the distinct edges of the features.

Phase imaging monitors the changes in phase offset, or phase angle, of the input signal to drive the piezo with respect to the phase offset of the oscillating cantilever. Photodiode detector has the role of comparing the phase of the drive signal to the phase of the cantilever response. The phase offset between the two signals when the cantilever oscillating freely in air is defined as zero. The phase offset of the oscillating cantilever changes by some angle with respect to the phase offset of the input drive signal, as the probe tip engages the sample surface. If elasticity of the sample surface changes from place to place in the scanning region, the damping of the probe tip varies as it raster across the sample surface. This results in the changes of the phase angle between the two signals. The plot of these differences is so-called phase image.

Photodiode detector can also monitor the amplitude of the cantilever. Amplitude map of the sample surface is plotted from the root mean square values of the laser signal on the y-axis of the detector which is recorded for all segments on a given raster of the probe tip. Edges of surface features tend to be shown well in amplitude images.[66,67]

3. Experimental details

Four different types of ssDNA-SWCNT hybrids were studies in this thesis. Nanocyl-Poly (CG), HiPCO-Poly (CG), Nanocyl-Poly (AT) and HiPCO-Poly (AT) Hybrids were prepared and characterized by IEX (HPLC), AFM and UV-Vis spectrometer. Table 3-1 gives the ssDNA sequences and the expected purified CNT chiralities by IEX. Since we were aiming to purify and work with thick SWCNTs, we have chosen these ssDNA sequences.[49]

Table 3- 1 ssDNA sequences that were used in this study and the SWCNT chiralities of the dominant hybrids.

ssDNA sequence	CNT chirality
$(TTTA)_3T$	(10,5)
$(CCG)_2CG$	(8,7)

3.1 DNA-CNT Hyprid Preparation

ssDNA stock was prepared from $(CCG)_2CG$ and $(TTTA)_3T$ ssDNA that were purchased from Sigma company. The final concentrations of Poly (CG), Poly (AT) ssDNA stocks (measured by UV-Vis spectrometer, Nanodrop) were 3.98397 and 3.9113 µg/µl respectively.

The samples were prepared by dissolving 1±0.1g SWCNT and 1g ssDNA in 1ml buffer called dispersion solution. Different buffers were made and used for various samples (see table 3-2).

Table 3- 2 Dispersion solutions used for ssDNA-SWCNT hybrid preparation.

Sample	Dispersion Buffer
Nanocyl-$(CCG)_2CG$	0.1 M NaCl, 10% glycerol
HiPCO-$(CCG)_2CG$	
Nanocyl-$(TTTA)_3T$	0.1 M sodium acetate pH 4.5
HiPCO-$(TTTA)_3T$	

Sodium acetate is an ionic compound with the chemical formula $C_2H_3NaO_2$ and it is often used as a buffer to keep a relatively constant pH. This is useful especially in biochemical applications where reactions are pH dependent.

Sonication is required for effective dispersion, similar to the conditions required for CNT dispersion by many surfactants.

During sonication the sample in the eppendorf tube was placed in a steel block inside a coolant reservoir. Ice bath condition is required to minimize sample evaporation.

Sonication was carried out by VC130PB sonicator. The parameters of the sonicator's program were set to get the average power of 8 watt. The program was set to pulse mode with 0.7seconds on and 0.1 sec off and the amplitude was set to 17%.

After sonication, we usually end up with about 800 µl of the sample in the tube. In the case of $(TTTA)_3T$ ssDNA, the sample were incubated for 2 days to give enough time for better interaction between $(TTTA)_3T$ ssDNA and SWCNT.

To well separate the big CNT bundles from the rest of the sample, the samples were aliquoted to volumes of 100 µl and centrifuged for 90 min with the speed of 16000 g. *MICROCL 17* Centrifuge was used for centrifugation. This leaves DNA dispersed nanotubes solution at a mass concentration in the range of 0.2-0.4 mg/ml which is suitable for IEX (HPLC) run.

Removal of free DNA by either anion exchange column chromatography or nuclease digestion does not cause nanotube flocculation, indicating that DNA binding to carbon nanotubes is very strong.

3.2 High Performance Liquid Chromatography of DNA-CNT hybrids

In this study *SHIMADZU* HPLC system was used for DNA-SWCNT separation. Figure 8 shows different parts of this setup. The maximum pressure that can be applied to this HPLC system is 300bar.

Figure 8 High Pressure Liquid Chromatography system used for sorting carbon DNA-CNT hybrids.

In this experiment two elution solutions were used for eluting the IEX column. The elution solution that was used for finding the baseline as well as for sample loading (Solution A) and the other for applying a salt gradient for the elution and separation of DNA-CNTs which are bound to the column after the loading process.

Solution A was prepared with sodium chloride, sodium citrate and EDTA to get the final concentrations of 0.3M, 0.03M and 0.5mM respectively. The pH of the solution was adjusted to 7. Salt concentrations and pH value are two factors that are highly important in the separation of hybrids and a slight shift in buffer pH may affect the retention of hybrids in the IEX column.

Solution B was prepared from solution A by adding sodium benzoate to get the final molarity of 1M. This process was done using 8 watt magnetic stirrer.

Sodium benzoate eluent is rather large organic anion that is less mobile than most inorganic anions and therefore have lower equivalent conductance. Molecular structure and IR spectrum of sodium benzoate was calculated by ChemBioDraw3D Ultra12.0 and shown in figure 9.
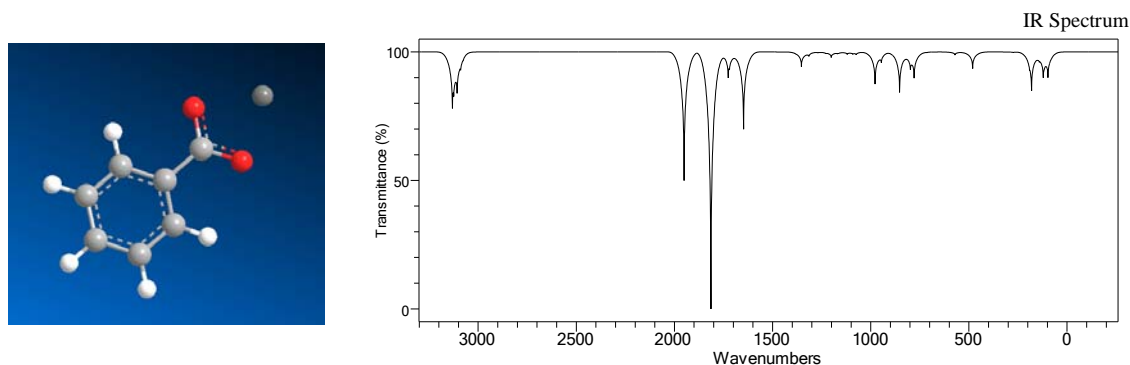
IR Spectrum

Figure 9 Molecular structure and IR spectrum of sodium benzoate.

Both solutions were purified by the filtering setup which is shown in Figure 10. The setup contains *MILLIPORE* membrane filter with 0.22 µm pore size and a high pressure pump.

In order to run the IEX chromatography, HYDROCELL CNT-NS 1500 column chromatography was mounted on the HPLC system. This column is produced from 10µm of highly cross-linked PS-DVB beads with pore diameter of 500 Å (See Figure 11).

Solution A and B were connected to the pumps of HPLC machine. Before each IEX experiment, the HPLC setup was running with solution A with a flow rate of 0.1 ml/min for overnight to make sure that the set up works properly and the column is clean enough.

Figure 10 Filtering system used for purification of elution solutions that were used in IEX process.

The stability and functioning of HPLC machine and the detectors were checked just before each sample injection. Diode array was the detector of the HPLC set up used in this study. This was done by recording the baseline with solution A and a flow rate of 1ml/min for about 20 to 30 minutes.

Figure 11 HYDROCELL CNT-NS 1500 column.

For sample injection special syringes were used.
To prevent any probable trouble in the column flow, the syringe was checked not to contain any air bubble. Taking into consideration that the loop volume is 1ml and the column size is 75×7.6mm, 18 minutes is enough for sample loading. The loading has been done using solution A with the flow rate of 2ml/min. At this stage it is expected that DNA and anything that is bound to it have bound to the resins in the IEX column, and everything else is eluted to the waste.

At the next step a gradient of 0-1 M of solution B is applied to the setup and sodium benzoate replaces DNA-CNT hybrids gradually. Eluted hybrids were collected and saved for further analysis. Each collected aliquot had a volume of 1 ml. During the elution diode array detector records UV-vis absorption spectra in the wavelength range of 290-800 nm.

After each experiment the column was washed with solution B for 30 minutes with the flow rate of 1ml/min. The column was prepared for storage after washing it with 15 ml of H_2O, 0.05% sodium azide. Sodium azide can prevent bacteria growth. The column can be stored in a 4 °C cold room.

Table 3-3 demonstrates the different ssDNA-CNT samples used for IEX separation of (8,7) and (5,10) CNTs. The HPLC set up was programmed to apply the salt gradient of 0 to 1 molar of solution B which contains sodium benzoate in the time period and elution rates mentioned in the table below.

Table 3- 3 Method used for IEX separation of ssDNA-CNT.

Experiment No.	Sample	Elution flow rate (ml/min)	Time period for elution gradient of solution B (min)
1	0.1 M NaCl, 10% glycerol (Control experiment)	1	20
2	0.1 M sodium acetate pH 4.5 (Control experiment)	1	20
3	Nanocyl-Poly(AT)	2	20
4	Nanocyl-Poly(CG)	2	20
5	HiPCO-Poly(CG)	2	40
6	HiPCO-Poly(CG)	2	20
7	HiPCO-Poly(AT)	2	20

3.3 Spectroscopic Characterizations of DNA-CNT hybrids

The UV-Vis measurements in this thesis were done by Perkin Elmer Lambda 850 UV-Vis spectrometer, driven by UVwin Lab 5.1 software.

The optical setup of the commercial UV-Vis spectrometer is given in Figure 12. As it is illustrated the beam splitter divides the laser beam to two separate branches that pass the sample compartment. In this section one beam passes the background and the other goes through the actual sample. Water was selected as the zero background in this study.
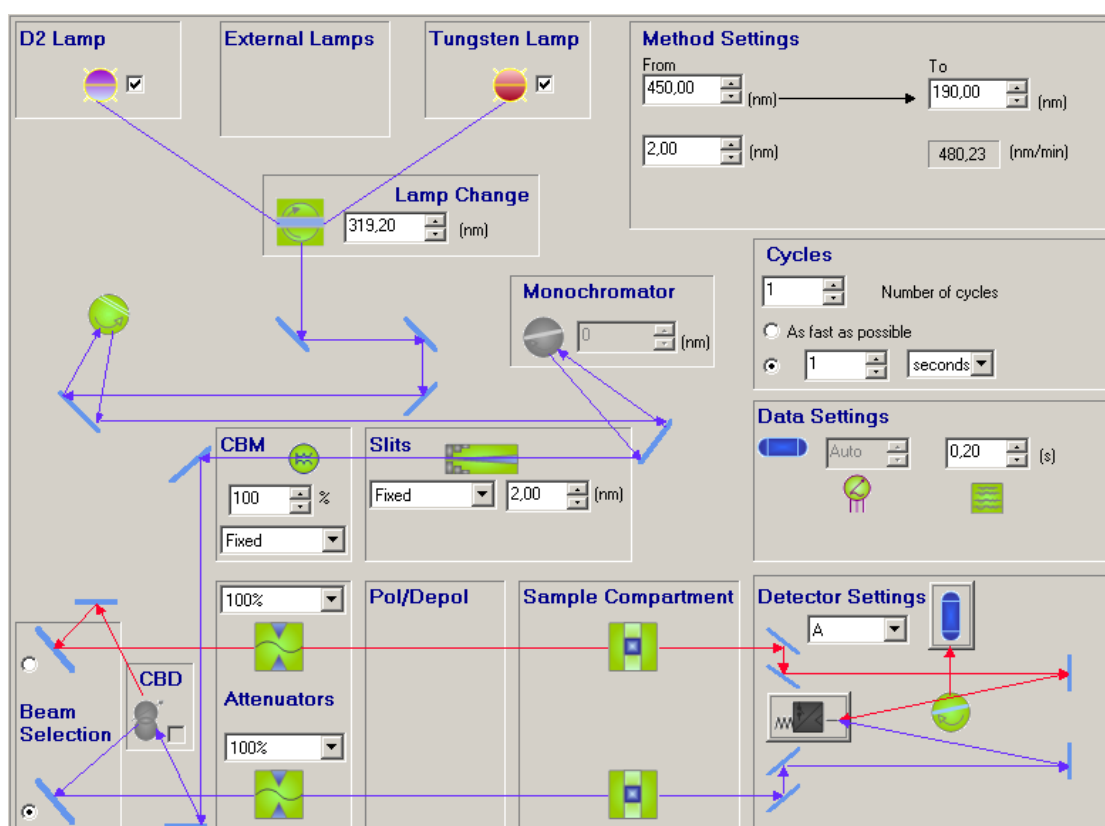
Figure 12 Schematic diagram of laser path in UV-Vis spectroscopy setup.

1 ml quartz cuvettes were used for the measurements. The total volume of 900 µl was pipetted to the quartz cuvettes. The first step was to measure the auto zero for system calibration. This was done by placing water in both channels of the spectrometer. The blank for each sample was corresponding buffer used in that sample. Table 3-4 shows the samples that were prepared for this purpose.

Table 3- 4 Samples prepared for UV-Vis spectroscopy. The percentages are the ratio of the sample diluted in the corresponding buffer solution.

Sample	Preparation	Sample	Preparation
Solution A	100%	Fraction 20 taken from IEX of HiPCO-(CCG)$_2$CG	100%
Solution B	100%	Fraction 21 taken from IEX of HiPCO-(CCG)$_2$CG	100%
0.1 M NaCl, 10% glycerol	100%	Fraction 22 taken from IEX of HiPCO-(CCG)$_2$CG	100%
0.1 M sodium acetate pH 4.5	100%	Fraction 23 taken from IEX of HiPCO-(CCG)$_2$CG	100%
Nanocyl-(CCG)$_2$CG before chirality sorting	10%	HiPCO-(TTTA)$_3$T before chirality sorting	10%
Nanocyl-(TTTA)$_3$T before chirality sorting	10%	Fraction 18 taken from IEX of HiPCO-(TTTA)$_3$T	100%
Fraction 21 taken from IEX of HiPCO-(TTTA)$_3$T	100%	Fraction 19 taken from IEX of HiPCO-(TTTA)$_3$T	100%
HiPCO-(CCG)$_2$CG before chirality sorting	10%	Fraction 20 taken from IEX of HiPCO-(TTTA)$_3$T	100%

3.4 Atomic Force Microscopic Characterization of DNA-CNT hybrids

We used AFM to further characterize the separated SWCNTs. Nanoscope V was the Atomic Force Microscope that was used for imaging ssDNA wrapped around SWCNT (see Figure 13). We decided to use Silicon AFM probes in these measurements. The tips had the spring constant of 40N/m and the resonant frequency of 300 kHz. The tip length and width were 125 µm and 40 µm respectively. The tips had the height of 14 µm and a radius less than 10µm.

The ssDNA-SWCNT samples prior IEX analysis and ssDNA-SWCNT from the separated fractions were deposited onto a piece of Silicon nitrate substrate. Furthermore, the control measurements were carried out with ssDNA and buffers. Tapping mode AFM (Digital Instruments multimode) was employed to acquire images of SWCNTs on the substrate under ambient conditions.
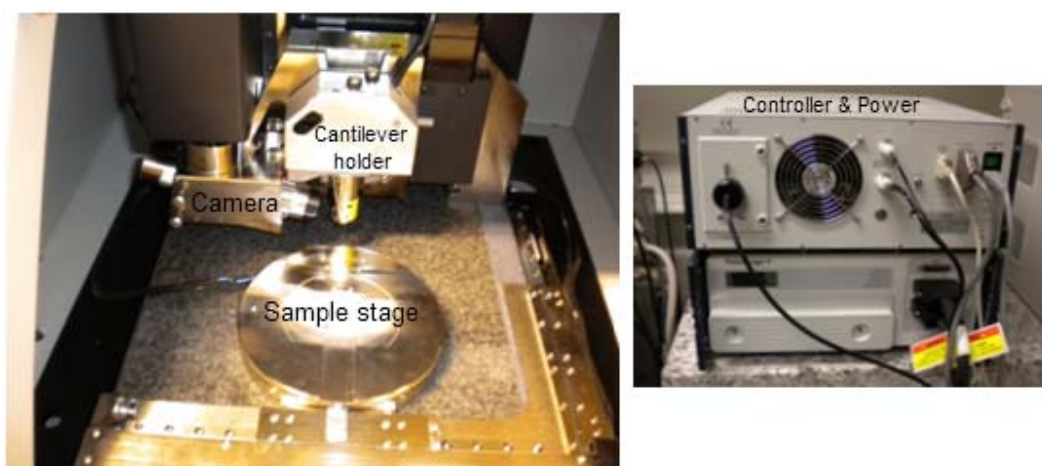
Figure 13 Nanoscope V. Schematic view of different parts of AFM setup used for characterization of DNA-CNT. Right: Controller, laser power and stage power systems, Left: sample stage, detectors and AFM tip holder.

Deposition of the samples were done by spin coating to apply uniform thin film of the samples to the wafer. The spin coater acceleration rate was set to 20 seconds and other deposition parameters for different samples are given in table 3-5.

Table 3- 5 Sample preparation parameters for AFM measurements.

Sample	No. of droplets	Spin Velocity (rpm)	Time (sec)
Solution A	15	1500	60
Solution B	15	1500	60

20 µl Poly (CG) and 100 µl Dispersion solution	2	2500	90
20 µl Poly (AT) and 100 µl Dispersion solution	2	2500	90
Nanocyl-$(CCG)_2CG$ before chirality sorting	1	4000	90
Fraction 23 taken from IEX of Nanocyl-$(CCG)_2CG$	15	1500	60
Nanocyl-$(TTTA)_3T$ before chirality sorting	2	4500	90
Nanocyl-$(TTTA)_3T$ before chirality sorting	1	3500	90
Nanocyl-$(TTTA)_3T$ before chirality sorting	1	2500	90
Nanocyl-$(TTTA)_3T$ before chirality sorting	1	1500	90
Fraction 24 taken from IEX of Nanocyl-$(TTTA)_3T$	15	1500	90
HiPCO-$(CCG)_2CG$ before chirality sorting	1	2500	90
Fraction 20 taken from IEX of HiPCO-$(CCG)_2CG$	20	1500	90
HiPCO-$(TTTA)_3T$ before chirality sorting	1	2500	90
Fraction 19 taken from IEX of HiPCO-$(TTTA)_3T$	20	1500	90

4. Results and Discussions

This chapter begins with presenting the results for successful preparation of 4 different samples, including Nanocyl-Poly (AT), Nanocyl-Poly (CG), HiPCO-Poly (CG) and HiPCO-Poly (AT), followed by results from purification of (8,7) and (10,5) CNTs of the mentioned samples by IEX method. As you will see chirality separation Nanocyl-ssDNA were weak, however the separation for HiPCO CNTs was very efficient. In the rest of this chapter fractions collected from IEX separation of HiPCO-Poly (AT) and HiPCO-Poly (CG) that contain highly purified (10,5) and (8,7) respectively were characterized by UV-Vis spectroscopy and atomic force microscopy.

4.1 Preparation of DNA-CNT

After the procedures for DNA-CNT hybrid preparation are done, the sample look like a homogeneous black solution (Figure 14). Homogeneity of the resulting sample indicates the role of hybrid in solubilizing CNTs in aqueous solutions. The solution was quite stable and I observed no precipitation for weeks.

The ssDNA-SWCNT preparations were then analyzed by Atomic force microscopy.
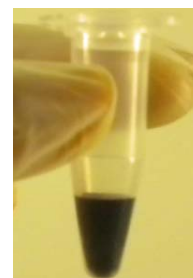
Figure 14 ssDNA-SWCNT hybrids before IEX.

4.1.1 Atomic Force Microscopy of ssDNA- Dispersion Solution

The imaging of $(CCG)_2CG$, 0.1 M NaCl, 10% glycerol and -$(TTTA)_3T$, 0.1 M sodium acetate pH 4.5 deposited on silicon nitride chips, were done as control, and to have reference for imaging of Poly(CG)-SWCNT and Poly(AT)-SWCNT respectively. In figure 15, AFM images of $(CCG)_2CG$, 0.1 M NaCl, 10% glycerol control chips demonstrate a very uniform pattern. Round-shaped aggregations of ssDNA can also be seen but with very few occurrences per 10 μm^2. The AFM measurements of deposited $(TTTA)_3T$, sodium acetate which is in agreement with our previous findings, also look like a uniform pattern.
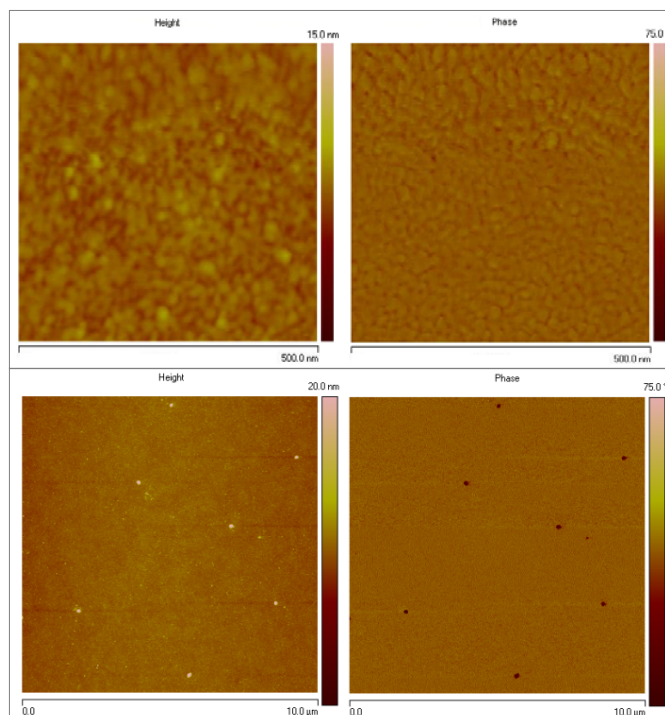
Figure 15 AFM images of single stranded Poly (CG) in its dispersion solution. Two left panels are height and phase images of 500 nm scan and the two right panels are height and phase images of a 10 µm scan.

A surprising finding in this study is that, in a certain region, (TTTA)$_3$ formed round shape aggregates and these round shape aggregations were located next to each other in a line. Figure 16 shows this region in the 10µm and 1.5µm scans.
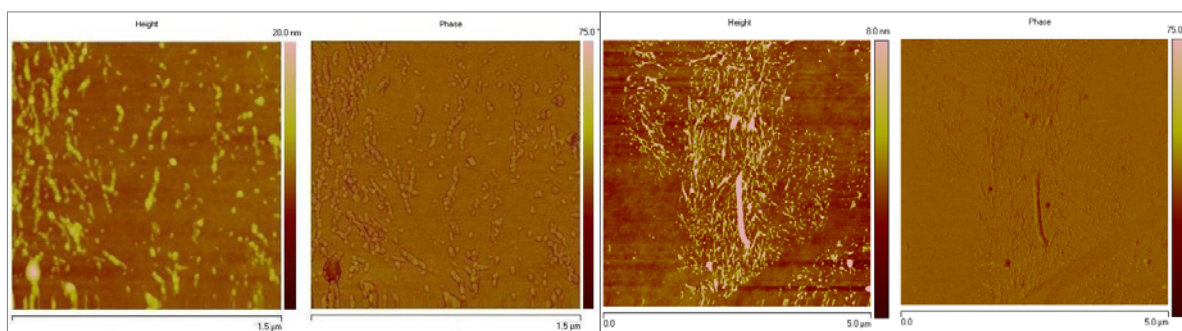

Figure 16 AFM images of single stranded Poly (AT) in its dispersion solution.

4.1.2 Atomic Force Microscopy of Nanocyl-Poly(AT) hybrids

The Nanocyl-Poly (AT) hybrid preparation was also analyzed and confirmed by AFM. Figure 17 shows the strong role of ssDNA in dispersing SWCNT in aqueous solution. Determination

of tube diameter results in the average diameter of 2.25 nm with the standard deviation of 0.83 nm. This clearly shows that bundle formation is prevented and existing bundles were destabilized upon hybrid formation.
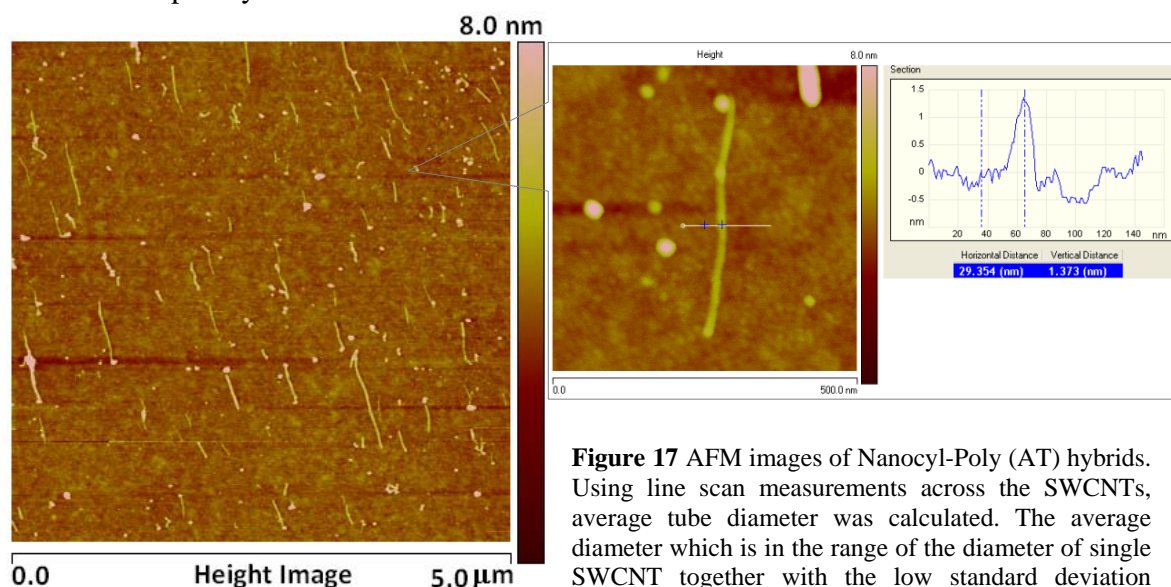
Figure 17 AFM images of Nanocyl-Poly (AT) hybrids. Using line scan measurements across the SWCNTs, average tube diameter was calculated. The average diameter which is in the range of the diameter of single SWCNT together with the low standard deviation explains the nonexistence of bundles.

4.1.3 Atomic Force Microscopy of Nanocyl-Poly(CG) hybrids

AFM imaging of Nanocyl-Poly (CG) samples was not possible. Most probably the reason was the contamination of silicon nitride chip surface caused by the sample. To confirm that, the electron beam lithography was applied to create sharp rectangular nanoscale features and sample was deposited on that. Reduced sharpness of the features in the AFM images affirms the surface contaminations (see figure 18).
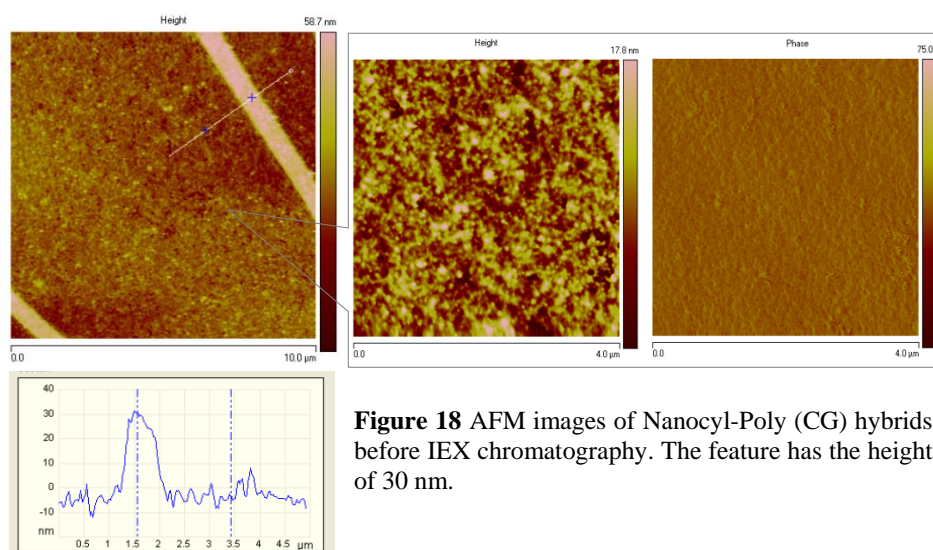
Figure 18 AFM images of Nanocyl-Poly (CG) hybrids before IEX chromatography. The feature has the height of 30 nm.

### 4.1.4 Atomic Force Microscopy of HiPCO-Poly(CG) hybrids

AFM images of HiPCO-Poly (CG) further show the effective role of ssDNA in dispersing SWCTTs and hindering SWCNT bundle formation. Figure 19, illustrates the images of HiPCO-Poly (CG) with two different scan sizes of 3 µm and 500 nm.
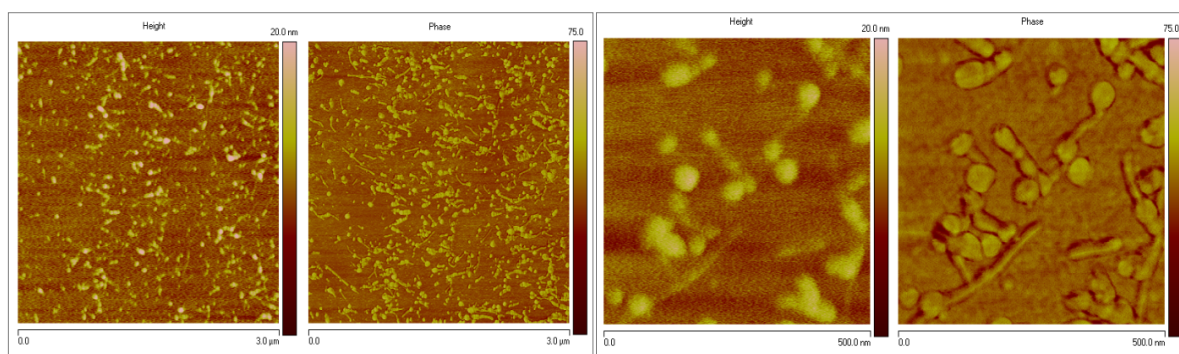
Figure 19 AFM images of HyPco-Poly (CG) hybrids before IEX chromatography.

### 4.1.5 Atomic Force Microscopy of HiPCO-Poly(AT) hybrids

Deposited HiPCO-Poly (AT) silicon nitride chips were imaged by AFM. Two different 500 nm size phase images in addition to one 10 µm scan are presented in Figure 20. The diameters of SWCNTs were measured by a line scan in the direction perpendicular to the tube axis. The measured average diameter of about 1 nm and the standard deviation of 0.39 signify that there is no bundle of SWCNTs and hence hybrid preparation was successful.
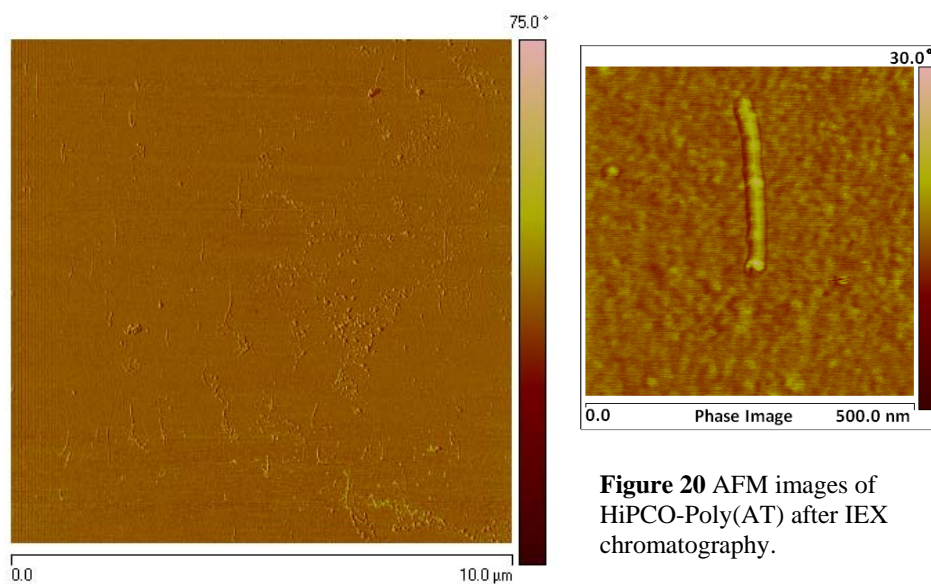
Figure 20 AFM images of HiPCO-Poly(AT) after IEX chromatography.

## 4.2 Ion exchange chromatography of ssDNA-SWCNT

The base line measurements were recorded before each IEX experiment to ensure that the HPLC setup was stable enough. Figure 21 is an example of the baseline measurement before sample injection in Poly (AT)-Nanocyl experiment. The absorption spectra were taken from excitation range of 200-800 nm in 30 minutes while solution A was eluting the column.
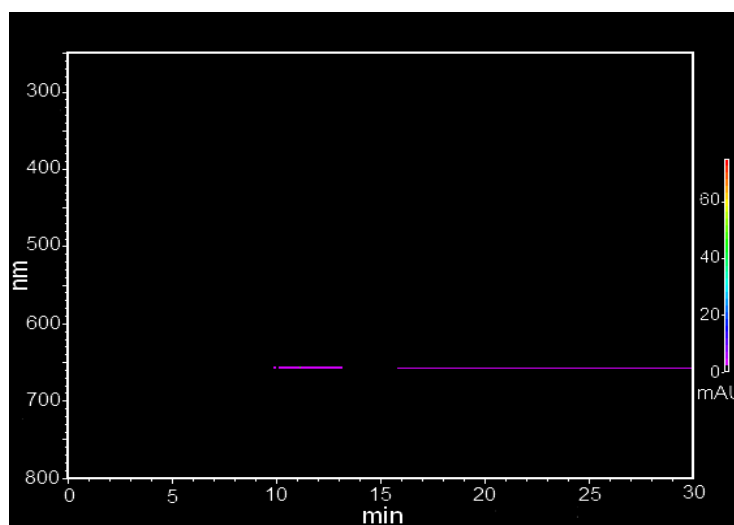
Figure 21 Electronic absorption spectra were measured to establish a baseline. Solution A was running with the flow rate of 1ml/min for 30min.

4.2.1   IEX Chromatography of NaCl, glycerol (Control experiment)

The control IEX experiment for Poly (CG)-SWCNT was done by injecting 200 µl of 0.1 M NaCl, 10% glycerol into the IEX column. The full spectrum and chromatogram of the loading process are illustrated in Figure 22.
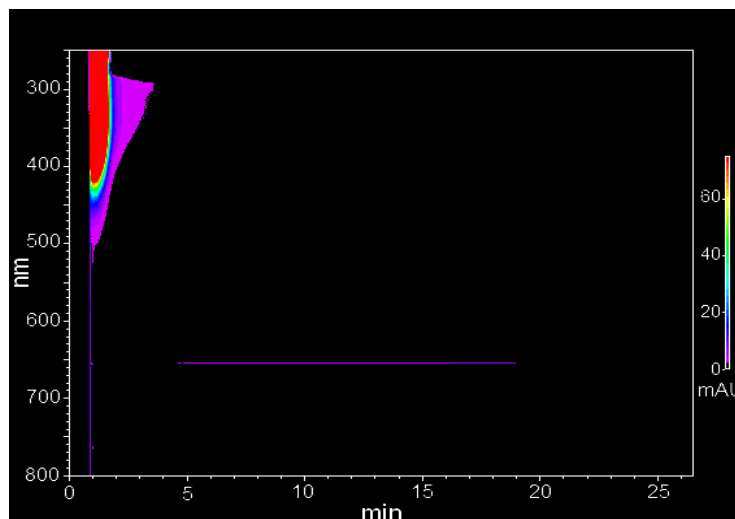
Figure 22 Chromatogram and the full spectra of loading volume of 200 µl of 0.1 M NaCl, 10% glycerol (the dispersion solution used as the medium of Poly(CG)-CNT) was injected into the anion exchange column NS1500. Intensity variation is illustrated with the color bar from black to red which corresponds to the range of 0-75 mAU.

Chromatogram of anion exchange separation of Poly (CG) -NaCl, glycerol is shown in Figure 23. The absorption spectra of the flow during this period were measured. The loaded sample was eluted according to the experiment No. 1 of Table 3-3.
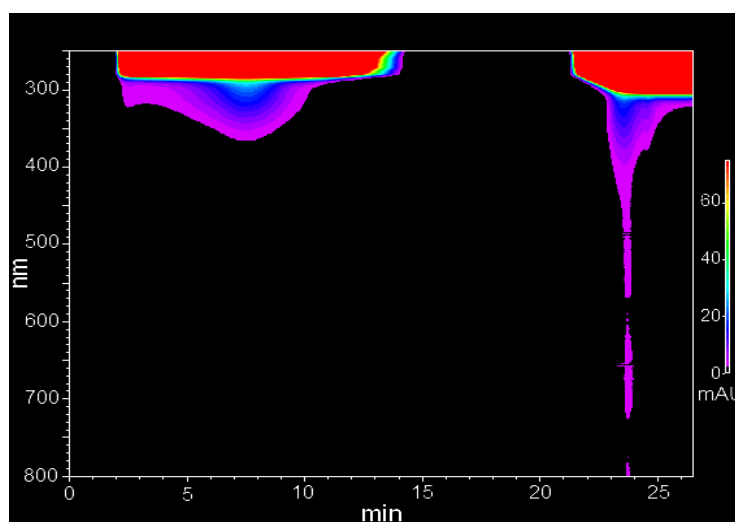
Figure 23 Chromatogram and the full spectra of elution process in the IEX of dispersion solution (control experiment of Poly (CG)-CNT). The linear gradient of sodium benzoate starts with 0% at t = 4 min and increases to 100% at t =24 min.

### 4.2.2 IEX Chromatography of sodium acetate (Control experiment)

In this experiment, 200μl of Sodium acetate (pH 7.0), (that is used as the medium for Poly (AT)-CNT) was infused into anion exchange column NS1500. The sample was loaded by solution A with the flow rate of 2 ml/min. The full spectra of the loading process are depicted in Figure 24.

Comparing the loading profile of two control experiments, differences between UV-Vis absorption peaks and elution chromatogram of some materials inside dispersion solutions are observable.
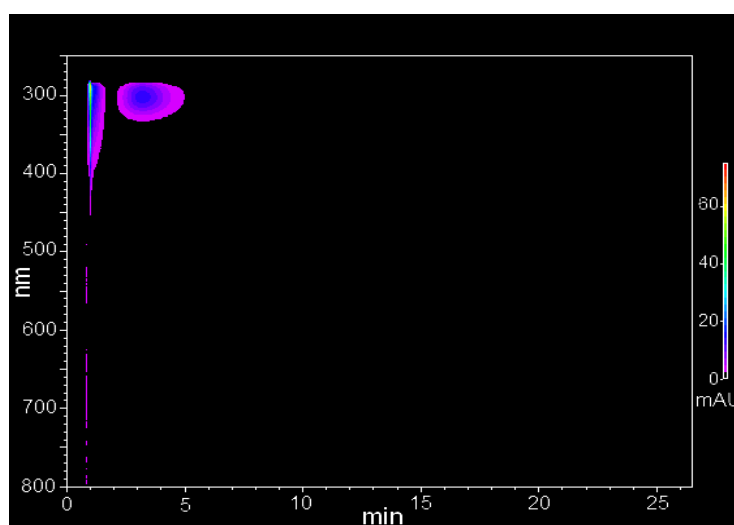
Figure 24 Chromatogram and the full spectra of loading volume of 200μl of sodium acetate that was injected in to IEX column.

Chromatogram of anion exchange separation of Poly (AT) in the corresponding dispersion solution is shown in Figure 2-15. The absorption spectra of the flow during this period were recorded. The volume of 40 ml of salt gradient was used for elution according to experiment No. 2 of Table 3-3.
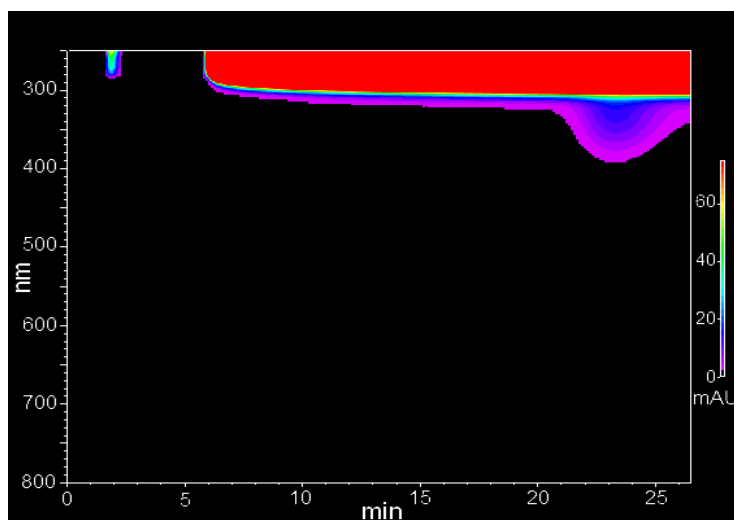
Figure 25 Chromatogram and the full spectra of elution process in the IEX of dispersion solution (control experiment of Poly (AT)-CNT). The linear gradient of sodium benzoate starts with 0% at t = 4 min and increases to 100% at t =24 min.

4.2.3   IEX Chromatography of Nanocyl-Poly(AT) hybrids

A volume of 200µl of Nanocyl-Poly (AT) was injected in to IEX column NS1500. The sample was loaded by solution A with the flow rate of 2 ml/min. The full spectra of the loading process are illustrated in Figure 26.
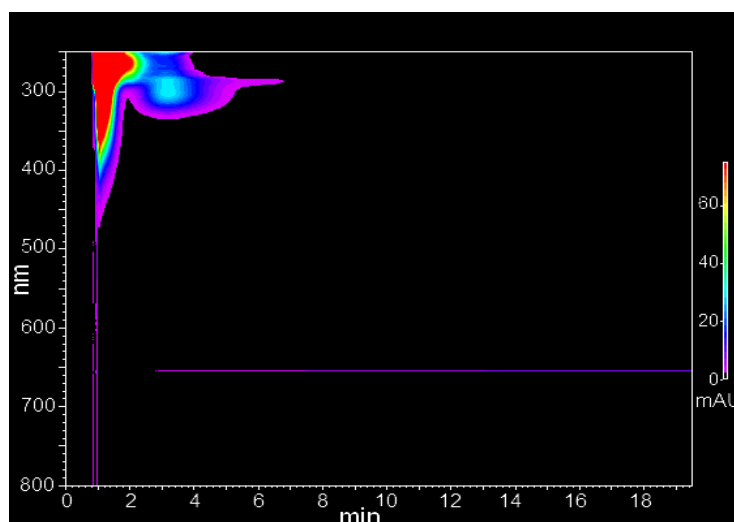

Figure 26 Chromatogram and the full spectra were measured to monitor the loading process 200µl of Poly (AT)-Nanocyl solution. The flow rate was 2 ml/min. Intensity variation is illustrated with the color bar from black to red which corresponds to the range of 0-75 mAU.

Chromatogram of anion exchange separation of Nanocyl-Poly(AT) is shown in Figure 27. The absorption spectra were taken from excitation range of 200-800 nm as a function of time. The broad absorption in wavelength at any time in the elution period shows the non specificity of the fractions and the presence of Nanocyl carbon nanotubes. The loaded sample was eluted with a linear salt gradient (0 to 1 M sodium benzoate at pH 7) in a 40 ml volume at a flow rate of 2 ml/min. Fractions were collected in 1 ml aliquots.
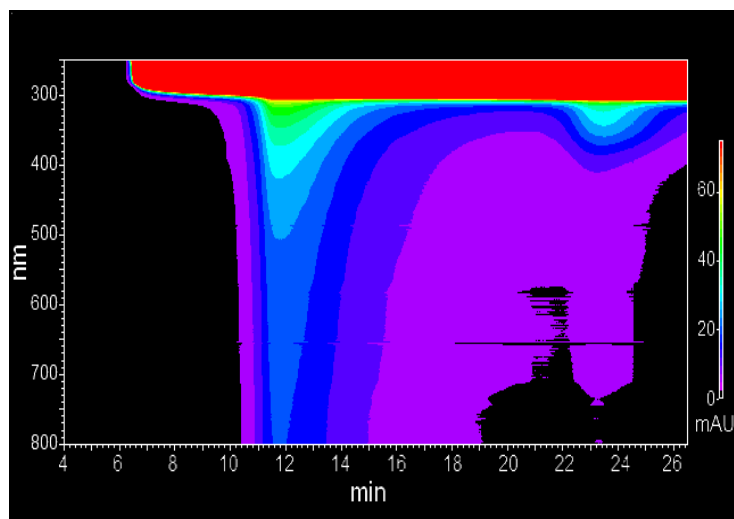

Figure 27 Chromatogram and the full spectra of elution process in the IEX control experiment of Poly (AT)-Nanocyl. The linear gradient of sodium benzoate starts with 0% at t = 4 min and increases to 100% at t =24 min.

The wide peaks in the chromatogram reveal the non efficient purification (Figure 28). When combined, the collected fractions gave an identical absorption spectrum to the starting material, indicating irreversible and nonspecific adsorption of DNA-CNT by the column.
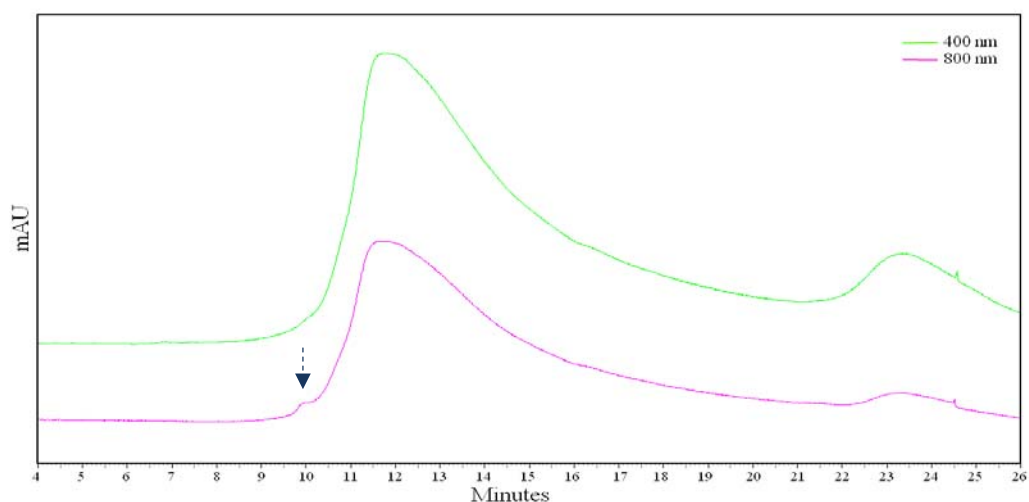
Figure 28 Chromatograms for elution process of the HPLC column in Nanocyl-Poly (AT) experiment. The first peak emphasized by the arrow, indicates the weak purification of (5,10) Nanocyl tubes.

Although non-specific separation of hybrids was detected in the elution process, Figure 28 shows that at t =9.91 min the concentration of hybrids of one kind of tubes were dominant. Looking at the UV-Vis spectrum taken by diode array of the IEX setup at this time and comparing that with previous (10,5) UV-Vis measurements [54], indicate that the two spectra are in agreement (see Figure 29).
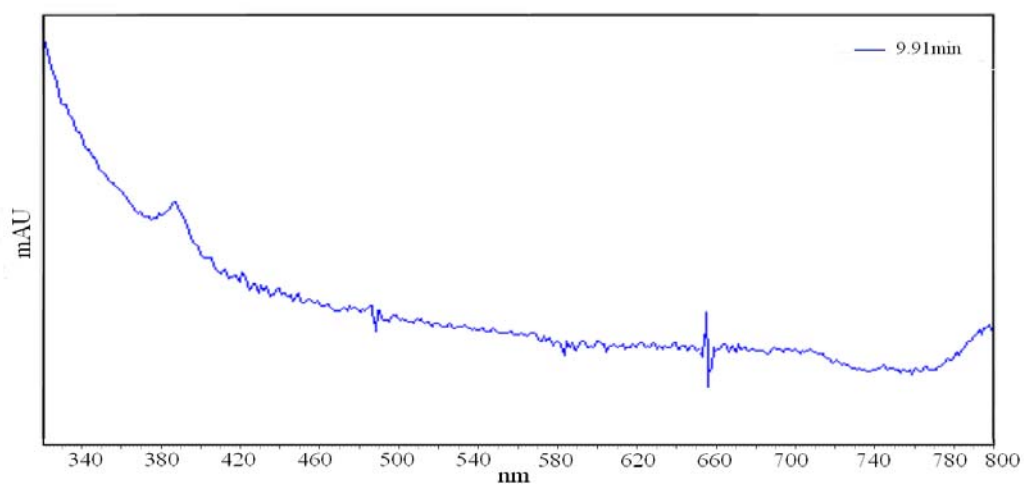
Figure 29 Electronic absorption spectra of Nanocyl-Poly (AT) at at t = 9.91 min in the IEX chromatography process.

High diameter variability of Nanocyl tubes is the main reason for non specificity of chirality and diameter sorting of Nanocyl-DNA hybrids (see Figure 30). Another potential reason for very low efficiency sorting of Nanocyl hybrids in both cases of $(TTTA)_3T$ might be the short length of these oligonucleotides compared to the circumference of the Nanocyl tubes. The

length of each Poly (AT) is 4.42 nm while the average diameter of Nanocyl tube is 2 nm. This can result in SWCNT non-structural oriented binding.
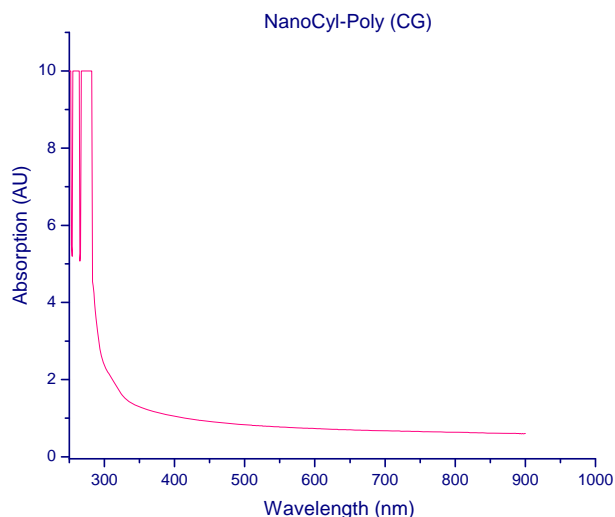
Figure 30 Spectrum taken by Ultra Violet-Visible spectrometer of Nanocyl-Poly (AT) solution before IEX chromatography.

4.2.4   IEX Chromatography of Nanocyl-Poly(CG) hybrids

A volume of 200µl of Nanocyl-Poly (CG) was injected into an anion exchange column NS1500. The sample was loaded by solution A with the flow rate of 2 ml/min. The full spectra of the loading process are illustrated in Figure 31.
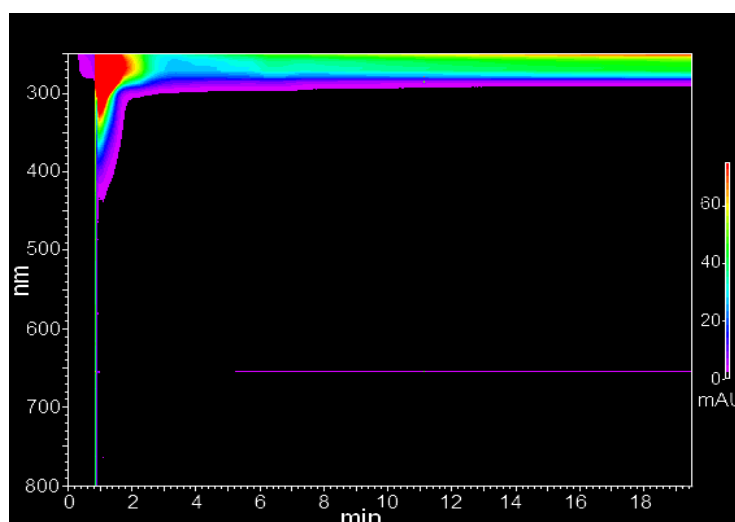
Figure 31 Chromatogram and the full spectra taken by diode array detector while loading 200µl of Nanocyl-Poly (CG) solution.

Chromatogram of anion exchange separation of Nanocyl-Poly(CG) is shown in Figure 32. The absorption spectra were taken from excitation range of 200-800 nm was plotted as a function of time. The existence of peaks indicates that the sorting method works. However, the broadness of adsorption band during elution is attributable to the non specific adsorption of the fractions and the presence of Nanocyl carbon nanaotubes. The loaded sample was eluted with a linear salt gradient (0 to 1 M sodium benzoate at pH 7) in a 40 ml volume at a flow rate of 2 ml/min. Fractions were collected in 1 ml aliquots. When combined, the collected fractions gave an identical absorption spectrum to the starting material, indicating irreversible and nonspecific adsorption of DNA-CNT by the column.
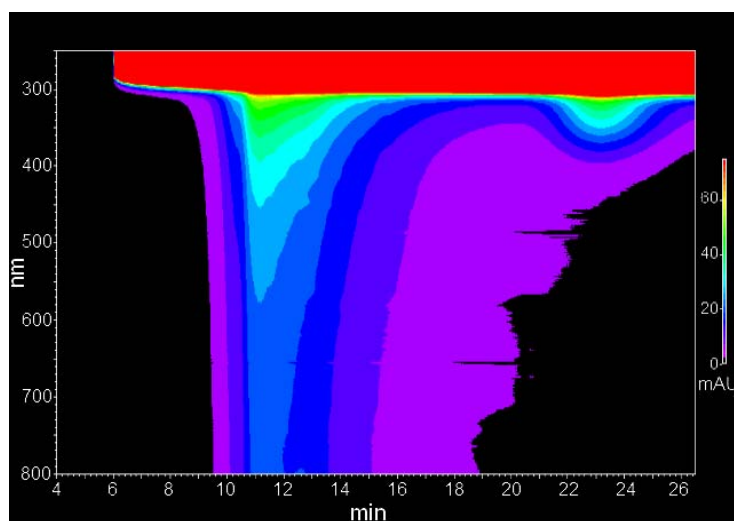

Figure 32 Chromatogram and the full spectra of elution process in the IEX control experiment of Poly (CG)-Nanocyl. The linear gradient of sodium benzoate starts with 0% at t = 4 min and increases to 100% at t =24 min.

Figure 33 indicates the elution profile of Poly (CG)-dispersed Nanocyl for the purification of (8,5) tube. The expected time for elution of this type of hybrids was at t=10.1 min which refers to the first shoulder seen in this figure.
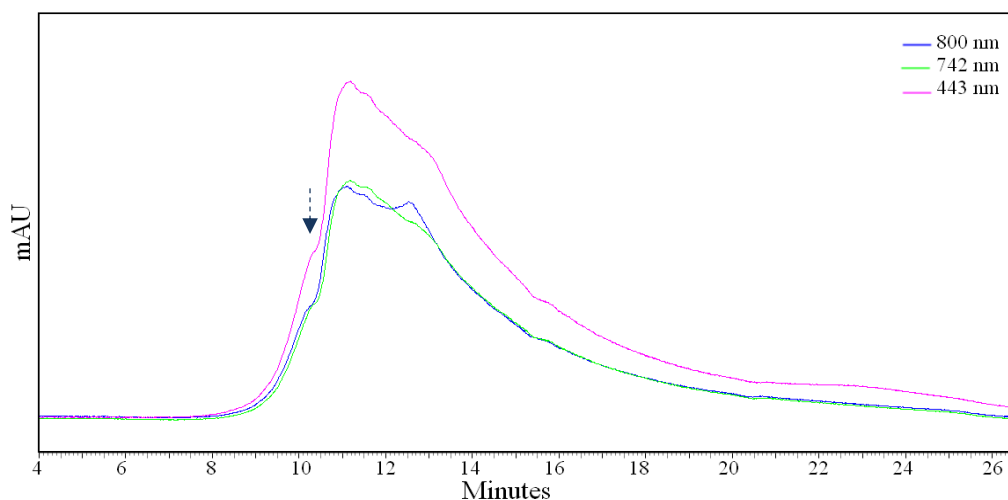
Figure 33 Chromatogram for elution process of the HPLC column in Nanocyl-Poly (CG) experiment.

Figure 34 shows that although non-specific separation of hybrids was detected in the elution process, at t = 13.14 min the concentration of hybrids with (8,7) tubes was dominant.
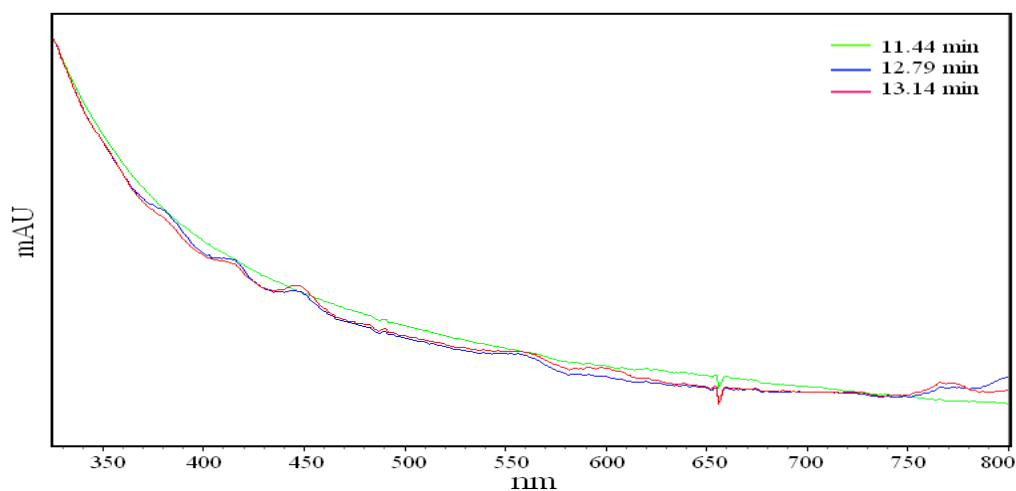
Figure 34 Spectrum taken during the IEX chromatography process of Nanocyl-Poly (CG) at t =11.44, t =12.79 and t =13.14 are shown in green, blue and red respectively.

Figure 35 is the UV-vis absorption measurements of Nanocyl-Poly (CG) before the IEX run. The high level of absorption intensity indicates the existence of CNTs (compare with control experiment intensities that the level of intensity was zero) however there is no peak visible resembling the absorption spectrum of Nanocyl-poly (AT) before IEX experiment.
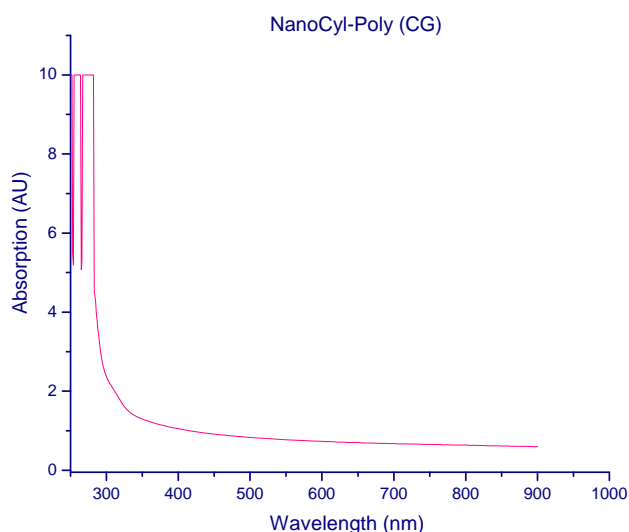
Figure 35 Spectrum taken by Ultra Violet-Visible spectrometer of Nanocyl-Poly (CG) solution before IEX chromatography.

One reason that the separation was not efficient, similar to the case of Nanocyl-poly (AT), is that the probability distribution of diameter in Nanocyl carbon nanotubes is very broad. This can also explain the absence of specific peak in the starting material's spectrum. The diameter variability of carbon nanotubes coming out from the IEX column simultaneously is high and therefore it is not possible to well separate hybrids based on their diameter and chirality.

In addition, the other reason might be due to the weak interaction between $(CCG)_2CG$ and Nanocyl that comes from the short length of the oligonucleotide (4.42), in comparison with the average diameter of nanocyl tubes which is 2 nm. This length is not enough for one pitch wrapping of the ssDNA around Nanocyl tubes.

4.2.5 IEX Chromatography of HiPCO-Poly(CG) hybrids

A volume of 200µl of HiPCO-Poly(CG) was injected into theIEX column. The sample was loading rate was 2 ml/min. Figure 36 shows the full spectra of the loading process.
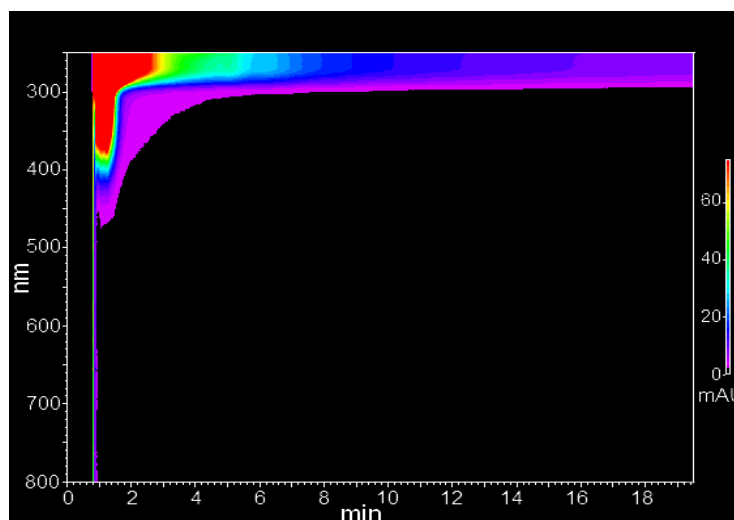
Figure 36 Chromatogram and the full spectra taken by diod-array detector of loading 200µl of HiPCO-Poly(CG) solution. The flow rate was 2 ml/min. Intensity variation is illustrated with the color bar from black to red which corresponds to the range of 0-75 mAU.

The loaded sample was eluted with a linear salt gradient (0 to 1 M sodium benzoate at pH 7) in a 40 ml volume at a flow rate of 2 ml/min. Fractions were collected in 1 ml aliquots.

Elution profile of Poly (CG)-dispersed HiPCO for the purification of (8,7) tubes were recorded (Figure 37).
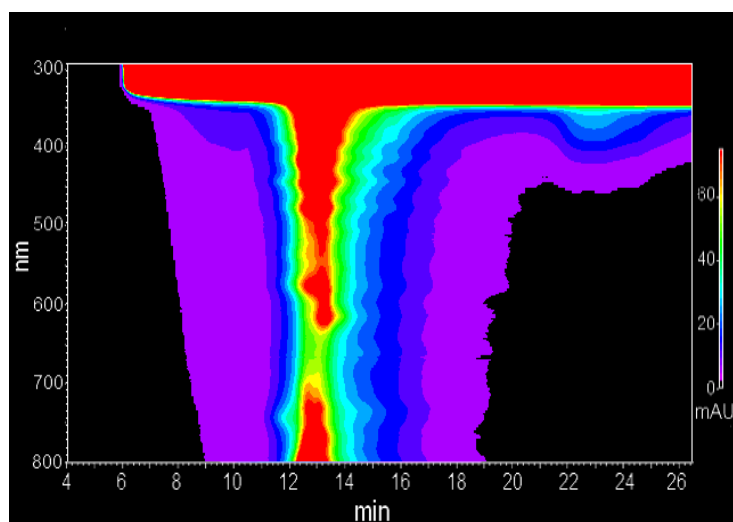
Figure 37 Chromatogram and the full spectra of elution process in the IEX control experiment of poly (CG)-HiPCO. The linear gradient of sodium benzoate starts with 0% at t = 4 min and increases to 100% at t =24 min.

It is noteworthy that part of the first shoulder corresponding to fraction collected at t = 11.45 min contains largely (8,7) tubes (Figure 38).
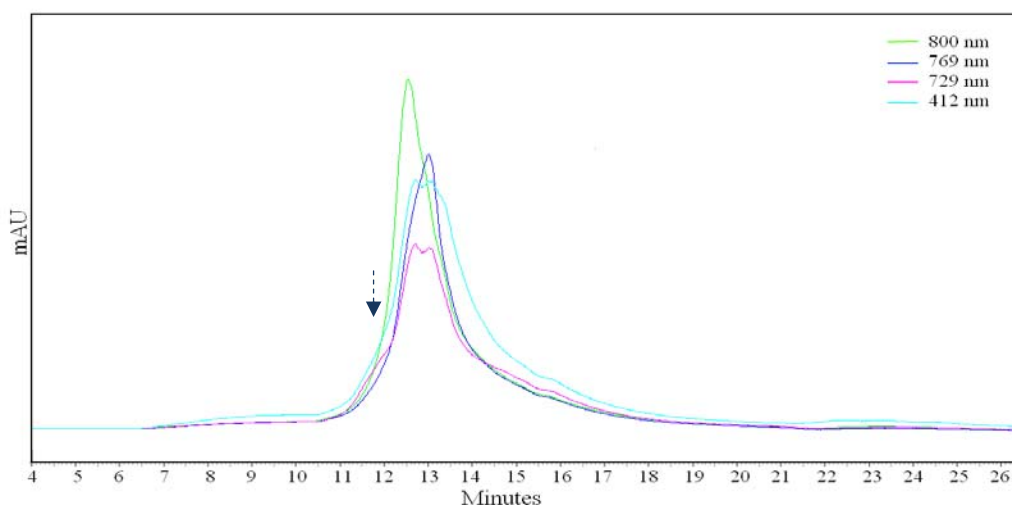

Figure 38 Chromatograms for elution process of the HPLC column in HiPCO-Poly (CG) experiment with standard gradient.

Absorption spectroscopy reveals a more quantitative analysis of the separation. Figure 39 shows the UV-vis absorption spectra of fractionated Poly (CG)-HiPCO. There are two transition regions identified in the spectrum first inter-band transitions for metals, M11 (400-650 nm) and second inter-band transitions for semiconductors S22 (550-900 nm).
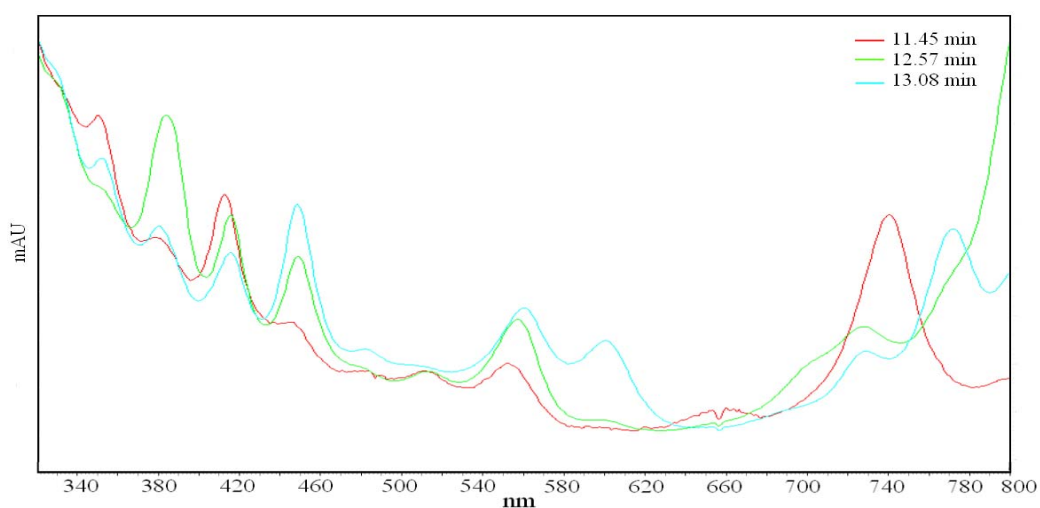
Figure 39 Electronic absorption spectra taken during the IEX chromatography process of HiPCO-Poly (CG) at t =11.45, t =12.57 and t =13.08 min are shown in red green and blue respectively.

For better separation of peaks of chromatogram, salt gradient of elution was optimized to starting from 0 M of sodium benzoate at t = 0 min rising to 1 M concentration at t = 44 min (Figure 40).
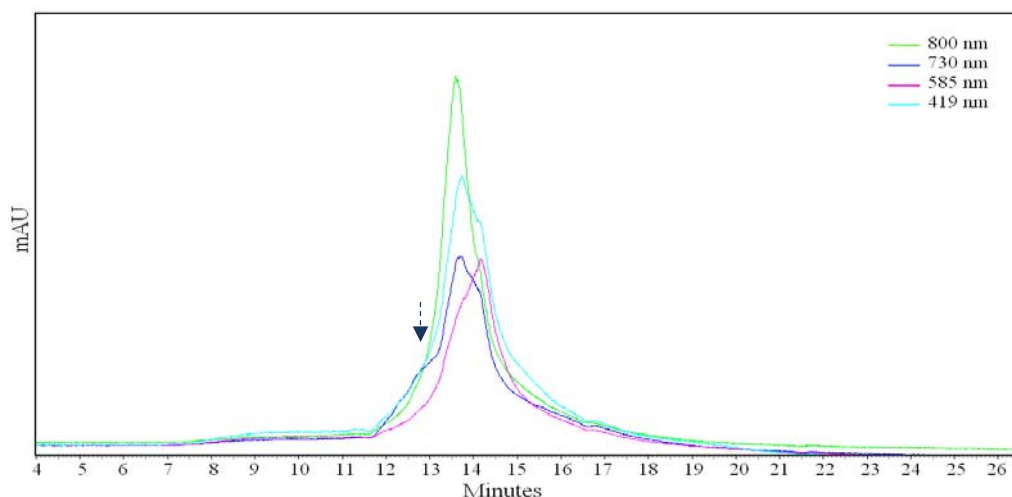
Figure 40 Chromatograms for elution process of the HPLC column in HiPCO-Poly (CG). The elution gradient was adjusted to reach the optimized separation.

4.2.6 IEX Chromatography of HiPCO-Poly(AT) hybrids

200µl of HiPCO-Poly (AT) was loaded in to IEX column NS1500 for HiPCO-Poly(AT) sorting by solution A with the flow rate of 2 ml/min. The full spectra of the loading process can be seen in Figure 41.
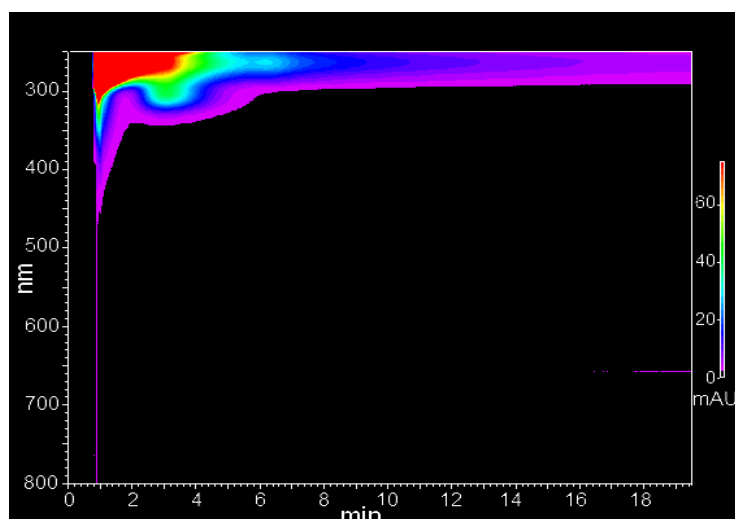
Figure 41 Chromatogram and the full spectra were measured to monitor the loading process 200µl of Poly (AT)-HiPCO solution.

Chromatogram of IEX separation of HiPCO-Poly (AT) is shown in Figure 42. The loaded sample was eluted with a linear salt gradient (0 to 1 M sodium benzoate at pH 7) in a 40 ml volume at a flow rate of 2 ml/min and aliquots of 1ml were collected.
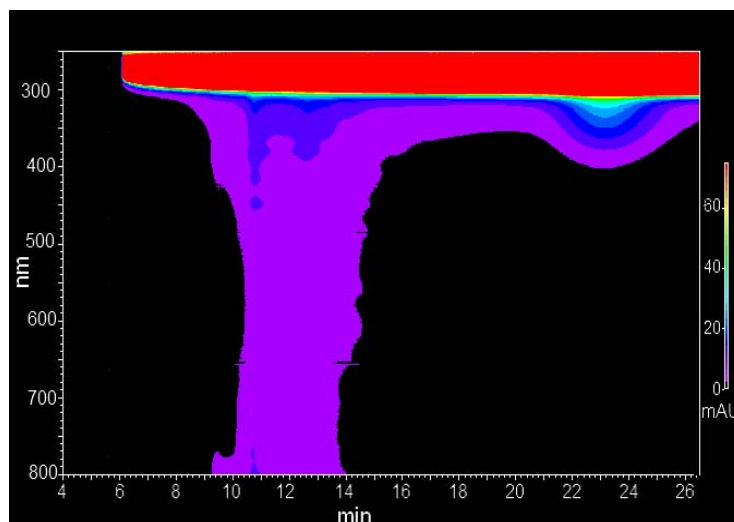
Figure 42 Chromatogram and the full spectra of elution process in the IEX control experiment of poly (AT)-HiPCO. The linear gradient of sodium benzoate starts with 0% at t = 4 min and increases to 100% at t =24 min.

As in the case of Poly (CG)-HiPCO, the peaks in the chromatogram of Poly(AT)-HiPCO are very narrow and sharp. Part of the first peak (in Figure 43) corresponding to fraction collected at 9.41 minute contains largely (10,5) tubes. Figure 44 shows optical absorption spectra of fraction that is enriched in (10,5) tubes.
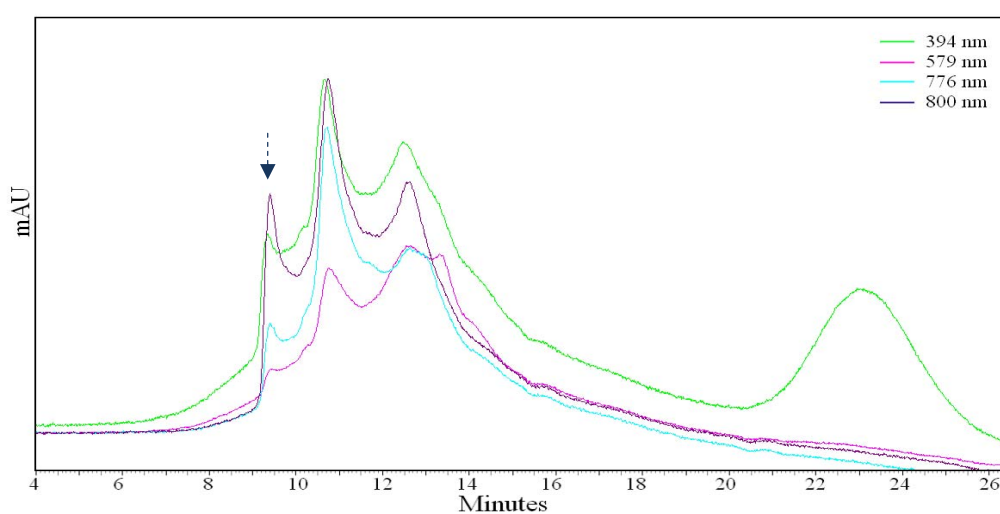
Figure 43 Elution profile of Poly (AT)-dispersed HiPCO for the purification of (10,5).
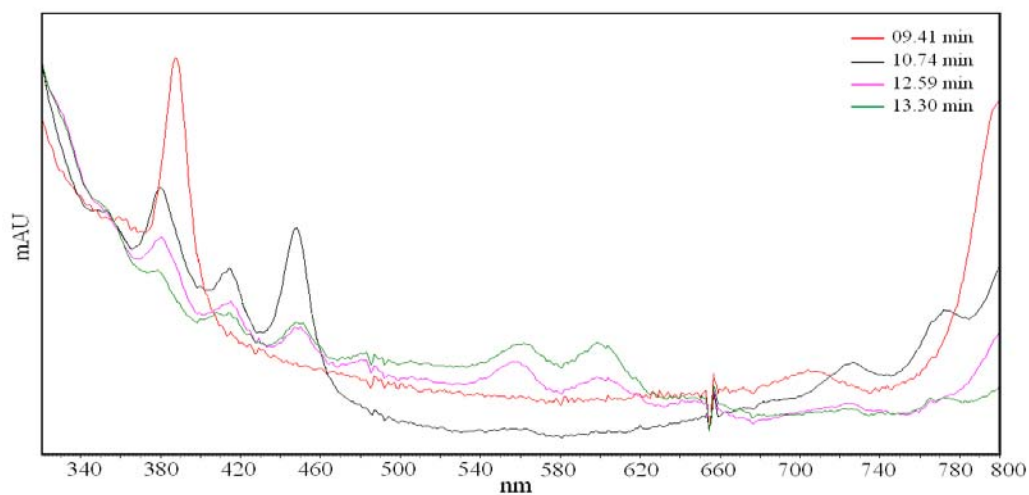
Figure 44 Electronic absorption spectra taken during the IEX chromatography process of HiPCO-Poly (AT) at t = 9.41, t = 10.74 and t = 12.95 and t= 13.30 min.

4.3 Optical Spectroscopy of DNA-CNT

As it was explained in the previous section, chromatograms taken from IEX separation of DNA-HiPCO samples, indicate their efficient separation. A visual comparison of the black starting material with fractionated materials of different color (light gray), immediately suggests that the CNTs have been sorted according to their electronic structures.

To verify the chirality purification, in this section detailed spectroscopic analysis of DNA-HiPCO after and before sorting and all the relevant control solutions are presented.
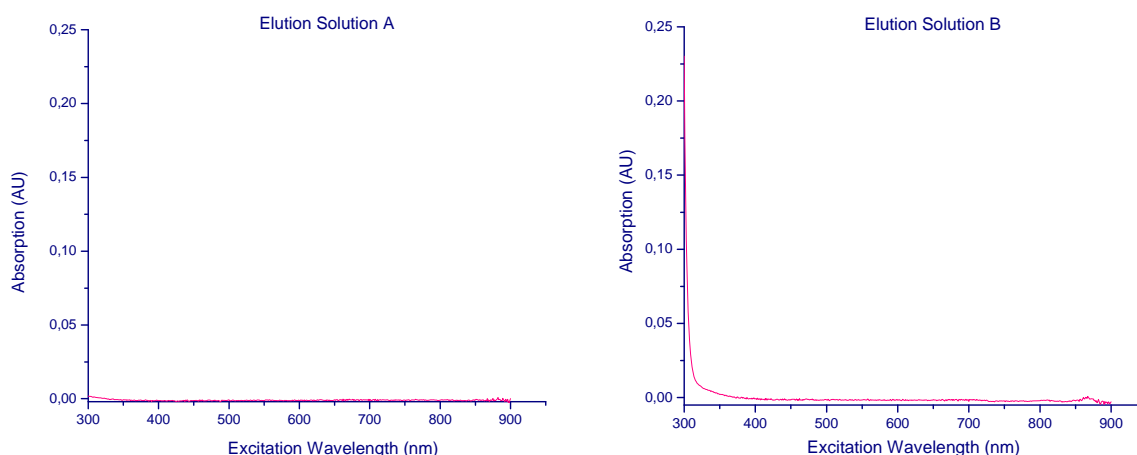
4.3.1   Optical Spectroscopy of Elution solutions

For characterizing the fractions, two important control measurements are UV-Vis spectral properties of solutions A and B. Here we demonstrate that these solutions do not have significant adsorption peaks that overlap with adsorption region of DNA-SWCNT hybrid (Figure 45).

Figure 45 Spectrum taken by Ultra Violet-Visible spectrometer of solution A and B are illustrated in left and right respectively.

4.3.2   Optical Spectroscopy of ssDNA-Dispersion solutions

In addition to elution solutions, some additional control measurements are essential. These are optical spectra of Poly (CG) and Poly(AT) in their corresponding dispersion solutions, 0.1 M NaCl, 10% glycerol and 0.1 M sodium acetate, respectively. The UV-vis absorption spectra of

these samples are given in Figure 46. The spectrum of Poly(CG)-SWCNT control sample does not have any absorption in the range of 300-900 nm and for the case of Poly (AT), only one sharp absorption peak at 290 nm was detected.
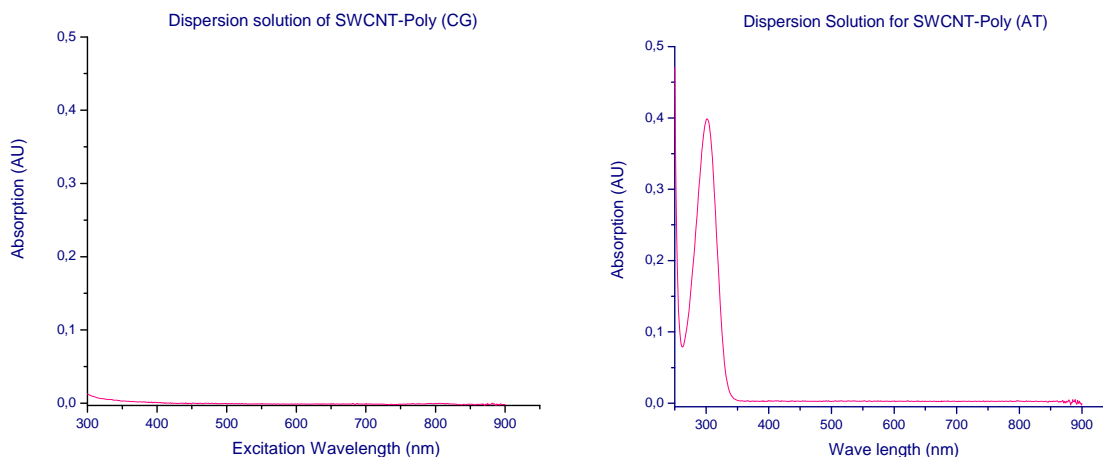
Figure 46 Spectrum taken by Ultra Violet-Visible spectrometer of (a) Poly (CG), 0.1 M NaCl, 10% glycerol and (b) Poly (AT), 0.1 M sodium acetate

4.3.3   Optical Spectroscopy of HiPCO-Poly(CG) hybrids

The starting material yields a spectrum typical of individually dispersed CNTs in aqueous solution, with multiple peaks arising from dissimilar types of CNTs overlapping across the full spectrum. Based on previous study we know that the signature peaks of (8,7) chirality are at wavelengths of 738, 411, 350 nm corresponding to E22, E33 and E44 transitions respectively.[54]

UV-vis measurements of the fractions were done. The absorption spectrum of one tube only contains the signature peaks of (8,7) chirality. The most (8,7) purified fraction was the one from tube No.22 . The absorption spectrum of starting material, fractions from tube No.22 and the neighboring tubes are shown in Figure 47.
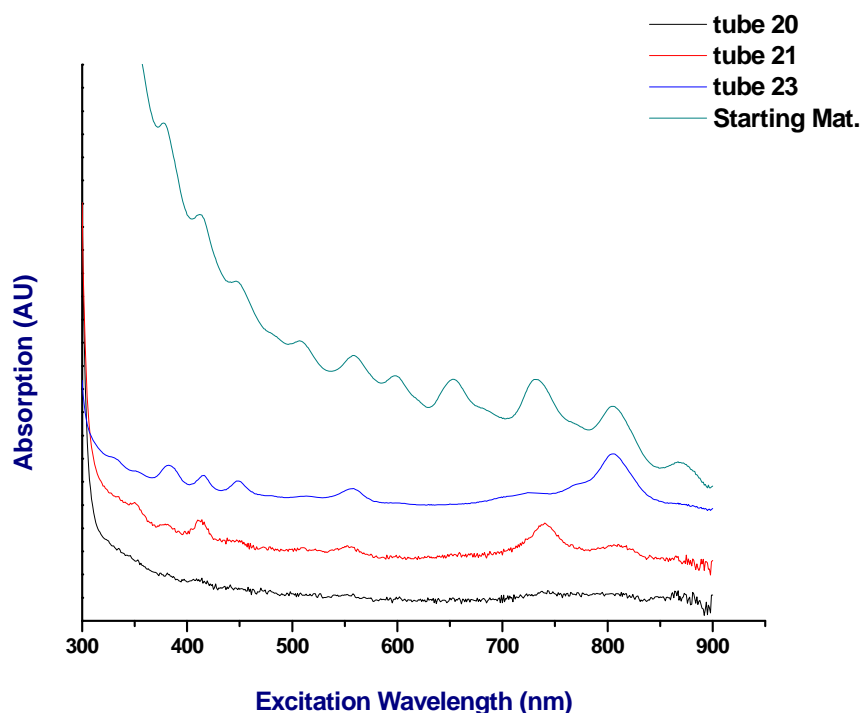
Figure 47 Spectrum taken by UV-Vis spectrometer of HiPCO-Poly (CG) solution before and after IEX chromatography. Tube 22 contains purified SWCNTs with (8,7) chirality.

4.3.4 Optical Spectroscopy of HiPCO-Poly(AT) hybrids

The UV-vis absorption of the HiPCO-Poly(AT) starting material and IEX fractions were also measured to verify the successful purification of the desired chirality, i.e. (10,5). Signature peaks of (10,5) in its spectrum, are reported to be at 795 and 386 nm corresponding to E22 and E33 transitions respectively.[54] The absorption spectrum of the IEX fraction analogous to tube No. 18 was found that perfectly matches the UV-vis spectrum of (10,5) CNTs (see Figure 48).
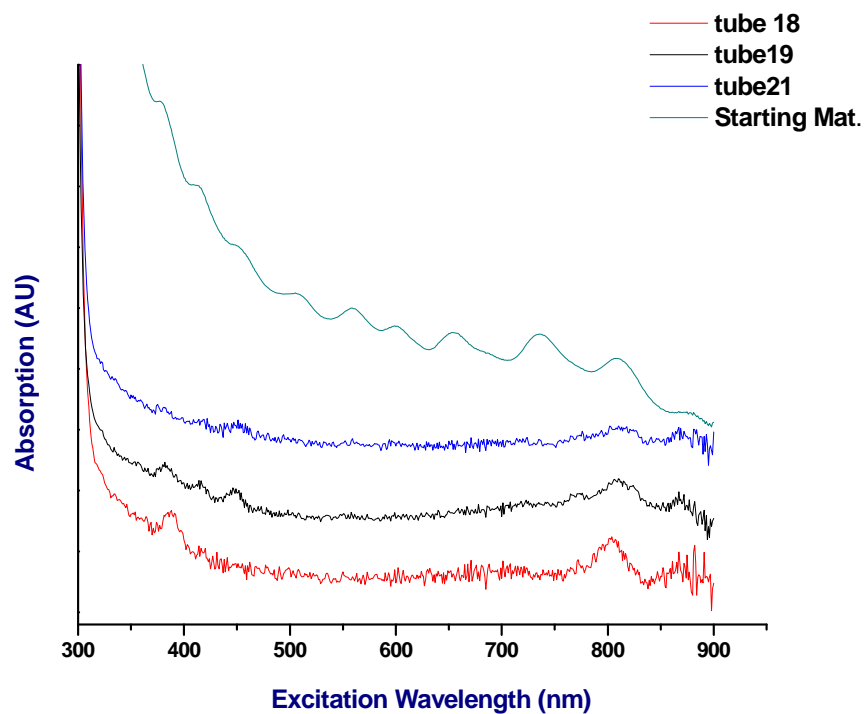
Figure 48 Spectrum taken by Ultra Violet-Visible spectrometer of starting material of HiPCO-Poly (AT) solution and fractions collected from IEX chromatography. Tube 18 contains highly purified (5,10) SWCNTs.

4.4 Atomic Force Microscopy of DNA-CNT

In this section, the result of AFM analysis of DNA-SWCNT is presented. Evidences from atomic force microscopy (AFM), support the results of UV-vis absorption spectroscopic characterization, confirming that hybrids do exist in the fractions and therefore the peaks in their absorption spectrum indeed originate from the hybrids.
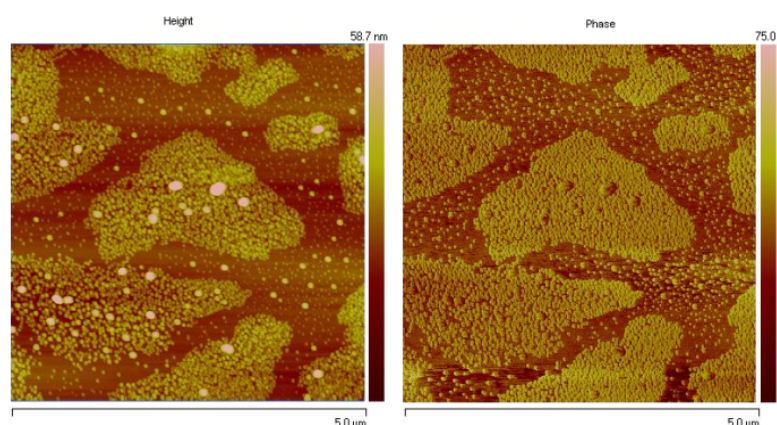
4.4.1   AFM imaging of Solution B

Taking in to account the control imaging results of section 1.1, the main control imaging that has to be considered for the AFM imaging of IEX fractions, is imaging the deposited solution B on a silicon nitride chip. The spherical particles shown in Figure 49 come from sodium benzoate salt in solution B. The particles are very clearly distinct and can be easily distinguished from CNTs or DNA aggregations. In addition the concentration of sodium benzoate in IEX fractions depends on the salt gradient at that time.

Figure 49 Atomic Force Microscopy image of solution B deposited on a silicon nitride wafer chip. Left and right panels show height and phase images respectively.

4.4.2   AFM imaging of IEX fraction of HiPCO-Poly(CG) hybrid

IEX fractions of HiPCO-Poly (CG) hybrid sample was imaged by AFM. The images taken from one of the fractions is illustrated in Figure 50. Detected CNTs in the AFM images prove the existence of hybrids in the fractions of IEX.
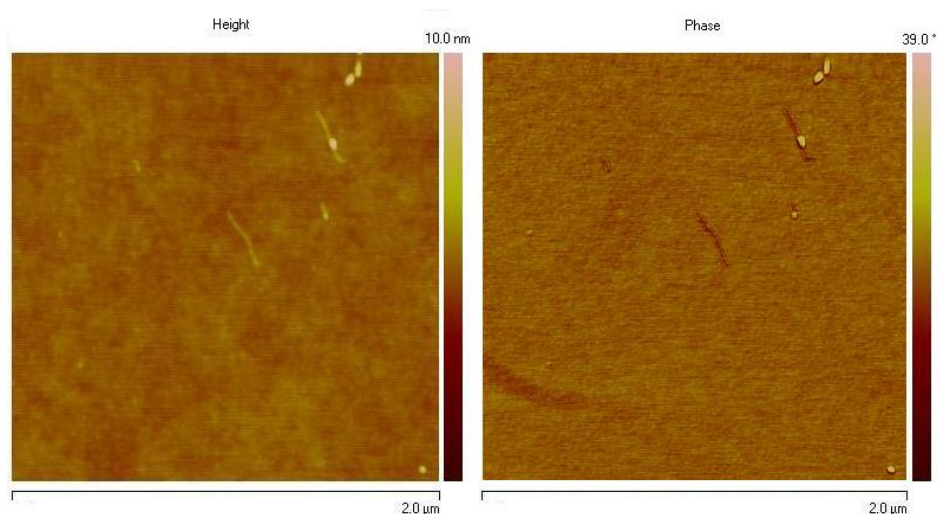
Figure 50 AFM images of HyPco-Poly (CG) hybrids. SWCNTs were observed in IEX fractions.

The detected hybrids had average diameter of 1 nm and average length of about 220 nm, as anticipated.

4.4.3 AFM imaging of IEX fraction of HiPCO-Poly(AT) hybrid

SWCNTs were indeed observed in IEX fractions of HiPCO-Poly (AT) as well. Line scans along the SWCNTs axis was studied. A very clear periodicity of about 20.8 nm with the standard deviation of 1.9 was detected. This periodicity suggests that DNA is wrapped around CNTs. To confirm that this periodicity does not come from the roughness of the surface, the line scan of the neighboring surface was done. Figure 51 shows that there is no such periodicity in the line scan of the surface.
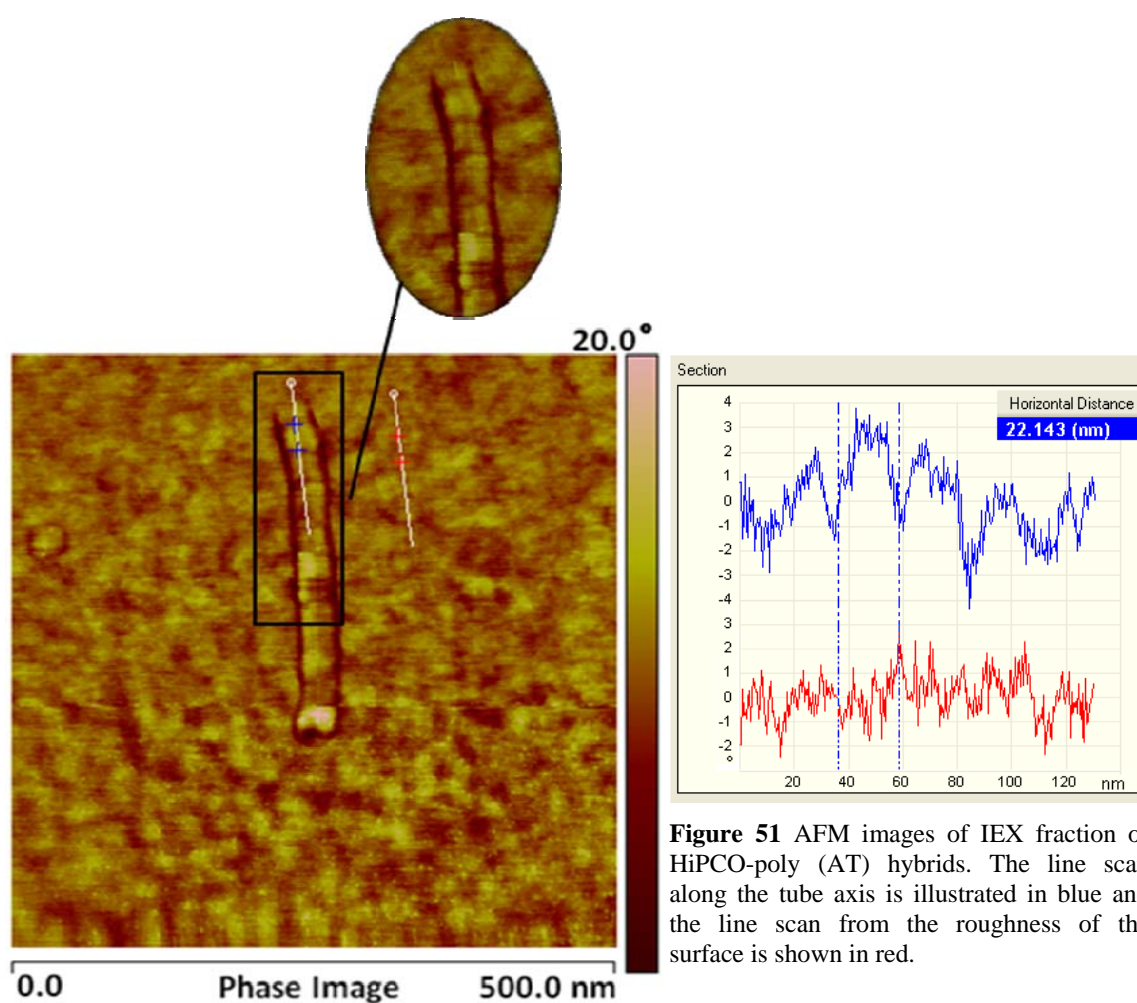
Figure 51 AFM images of IEX fraction of HiPCO-poly (AT) hybrids. The line scan along the tube axis is illustrated in blue and the line scan from the roughness of the surface is shown in red.

5. Conclusions

In nano electronics, where the device sizes are pushed towards sub-100 nm regime, we face several major challenges that originate from size scale of the system. One challenge is device size fluctuations that leads to a large variance in device characteristics. For example the threshold voltage and on/off currents fluctuate dramatically. A second challenge is the cost associated with nano fabrication.[68]

The solution to this problem is believed to lie in making use of recent advances in material science and supra molecular chemistry. For example by using carbon nanotubes (CNTs) and semiconductor nanowires, we can reduce the spread of the length scale, if we can control the diameters and other physical properties during the growth or chemical synthesis process. This control can in principle go beyond that achievable in top-down lithography.[69,70]

Electrical application of SWCNT is limited due to inhomogeneity of preparations. A SWCNT preparation can be used for electrical applications, if the tubes are dispersed and bundle formation is prevented. Another necessary condition is that the preparation has to be composed of tubes with equal chirality. This is because of the dependence of electrical properties on structure.

Inspired by recent developments in supramolecular chemistry, a protocol was developed for dispersing SWCNTs. The protocol is based on DNA-CNT self assembly and the dispersion relies on electric repulsion of negatively charged DNA backbones. In this thesis, ssDNA-SWCNT hybrids were successfully prepared and used as a method for dispersing and structural sorting of SWCNTs.

SWCNTs generated by HiPCO process, was dispersed homogeneously in aqueous solution. When original sample was spread on silicon nitride chips and analyzed by Atomic Force Microscope, a large number of tubes appeared as bundles even after vigorous sonication. Incubation of HiPCO tubes with ssDNA, destabilized the bundles. When the sample was spread on silicon nitride chips, individual nanotubes were observed and the number of tube bundles was substantially reduced.

The dispersed SWNT-DNA hybrid was stable on a very long time scales. Despite the homogeneity of the solution, the hybrid sample was structurally inhomogeneous. To achieve structural homogeneity, we took advantage of sequence dependent affinity of DNA for tubes with a given chirality. Using $(CCG)_2CG$ and $(TTTA)_3T$ oligonucleotides, we successfully sorted (8,7) and (10,5) HiPCO SWNTs using HPLC. We demonstrated structural homogeneity of the fractions, by optical absorption spectroscopy and Atomic Force Microscopy. In our spectroscopic investigation, we detected spectral signature of (8,7) and (10,5) HiPCO SWNTs. AFM analysis confirmed the presence of individual tubes with ssDNA wrapped around them.

We learned that efficiency of the chirality separation of SWCNT depends on the choice of synthesis protocol as well. Separation of Nanocyl is not as efficient as HiPCO. This can be explained by comparing the structure distribution probability of these two differently synthesized SWCNTs. The diameter distribution of Nanocyl is very broad while it is much narrower for the case of HiPCO (see section 2.1.2). On the other hand the lengths of ssDNA used for ssDNA-Nanocyl hybrid preparation might not be long enough for the purpose of high efficiency chirality separation of this type of tubes. Hence, in future oligonucleotides with repeated sequences of $(CCG)_2CG$ and $(TTTA)_3T$ could be used to potentially improve the purification efficiency of (8,7) and (10,5) Nanocyl SWCNT respectively.

The result of this study paved the way for electrical analysis and application of purified SWCNTs. In the next phase of this project, chirality purified SWCNTs will be used for TEM measurements on single SWCNTs deposited on e-beam fabricated silicon nitrate chips.

Finally, in view of the simplicity of formation and richness of DNA-CNT hybrid preparations, I hope that this study ignites interest in electrical and mechanical properties of DNA-CNT hybrids.

Bibliography

1. Kam, N. W. S. & Dai, H. Carbon Nanotubes as Intracellular Protein Transporters: Generality and Biological Functionality. *J. Am. Chem. Soc.* **127,** 6021–6026 (2005).

2. Chen, R. J. *et al.* Noncovalent functionalization of carbon nanotubes for highly specific electronic biosensors. *Proc. Natl. Acad. Sci. U.S.A.* **100,** 4984–4989 (2003).

3. Javey, A., Guo, J., Wang, Q., Lundstrom, M. & Dai, H. Ballistic carbon nanotube field-effect transistors. *Nature* **424,** 654–657 (2003).

4. Zheng, M. *et al.* DNA-assisted dispersion and separation of carbon nanotubes. *Nat. Mater.* **2,** 338-342 (2003).

5. Zheng, M. *et al.* Structure-Based Carbon Nanotube Sorting by Sequence-Dependent DNA Assembly. *Science* **302,** 1545 (2003).

6. McLean, R. S., Huang, X., Khripin, C., Jagota, A. & Zheng, M. Controlled two-dimensional pattern of spontaneously aligned carbon nanotubes. *Nano Lett.* **6,** 55 (2006).

7. Kam, N. W. S., O' Connell, M., Wisdom, J. A. & Dai, H. Carbon nanotubes as multifunctional biological transporters and near-infrared agents for selective cancer cell destruction. *Proc. Natl. Acad. Sci. U.S.A.* **102,** 11600 (2005).

8. Lustig, S. R., Jagota, A., Khripin, C. & Zheng, M. Theory of Structure-Based Carbon Nanotube Separations by Ion-Exchange Chromatography of DNA/CNT Hybrids. *J. Phys. Chem. B* **109,** 2559 (2005).

9. Endo, M. *PhD thesis* (Nagoya University, Japan, 1978).

10. Iijima, S. Helical Microtubules of Graphitic Carbon. *Nature* **354,** 56-58, (1991).

11. Kumar, S., *et al.* Synthesis, structure, and properties of PBO/SWNT composites. *Macromolecules* **35,** 9039-9043 (2002).

12. Coleman, J. N., Khan, U., Blau, W. J. & Gun'ko, Y. K. Small but strong: A review of the mechanical properties of carbon nanotube-polymer composites. *Carbon* **44,** 1624-1652 (2006).

13. Marquis, R., Supramolecular Discrimination of Carbon Nanotubes According to Their Helicity. *Nano Lett.* **8,** 1830–1835 (2008).

14. Ed. Chen,W. *Doped Nanomaterials and Nanodevices*, (American Scientific Publishers, Texas, 2007).

15. Huang, Z. P. *et al.* Growth of large periodic arrays of carbon nanotubes. *Appl. Phys. Lett.* **82,** 460-462 (2003).

16. Zhou, W. *et al.* Structural characterization and diameter-dependent oxidative stability of single wall carbon nanotubes synthesized by the catalytic decomposition of CO. *Chem. Phys. Lett.* **350,** 6-14 (2001).

17. Journet, C., Maser, W. K., Bernier, P., Loiseau, A., delaChapelle, M. L., Lefrant, S., Deniard, P., Lee, R. & Fischer, J. E. Large-scale production of single-walled carbon nanotubes by the electric-arc Technique. *Nature* **388,** 756-758, (1997).

18. Kokai, F., Koshio, A., Shiraishi, M., Matsuta, T., Shimoda, S., Ishihara, M., Koga, Y. & Deno, H. Modification of carbon nanotubes by laser ablation. *Diamond Relat. Mater.* **14,** 724-728 (2005).

19. *Nanocyl company, The carbon nanotube specialist,* http://www.nanocyl.com/en, 2011.

20. Nikolaev, P. *et al.* Gas-phase catalytic growth of single-walled carbon nanotubes from carbon monoxide *Chem. Phys. Lett.* **313,** 91–97 (1999).

21. Wong, E. W., Sheehan, P. E. & Lieber, C. M. Nanobeam mechanics: Elasticity, strength, and toughness of nanorods and nanotubes. *Science* **277,** 1971-1975 (1997).

22. Iijima, S., Brabec, C., Maiti, A. & Bernholc, J. Structural flexibility of carbon nanotubes. *J. Chem. Phys.* **104,** 2089-2092 (1996).

23. Hsu, H. L. *et al.* The synthesis, characterization of oxidized multi-walled carbon nanotubes, and application to surface acoustic wave quartz crystal gas sensor. *Mater. Chem. Phys.* **109,** 148-155 (2008).

24. Odom, T. W., Huang, J. L., Kim, P. & Lieber, C. M. Atomic structure and electronic properties of single-walled carbon nanotubes. *Nature* **391,** 62-64, (1998).

25. Girifalco, L. A., Hodak, M. & Lee, R. S. Carbon nanotubes, buckyballs, ropes, and a universal graphitic potential. *Phys. Rev. B* **62,** 13104 (2000).

26. Hirsch, A. & Vostrowsky, O. Functionalization of carbon nanotubes. *Functional Molecular Nanostructures* **245,** 193-237 (2005).

27. Meyyappan, M. *Carbon nanotubes science and applications* (CRC Press: Boca Raton, FL, 2005).

28. Javey, A., Guo, J., Wang, Q., Lundstrom, M. & Dai, H. *Nature* **424** 654 (2003).

29. Robinson, J. A., Snow, E. S., Badescu, S. C., Reinecke, T. L. & Perkins, F. K. Role of Defects in Single-Walled Carbon Nanotube Chemical Sensors. *Nano Letters* **6,** 1747-1751 (2006).

30. Ke, C.H., Pugno, N., Peng, B. & Espinosa, H.D. Experiments and modelingof carbon nanotube-based NEMS devices. *J. Mech. Phys. Solids* **53,** 1314 (2005).

31. Javey, A. *et al.* Carbon Nanotube Field-Effect Transistors with Integrated Ohmic Contacts and High-κ Gate Dielectrics. *Nano Lett.* **4,** 447 (2004).

32. Zheng, Q., Jiang, Q., Multiwalled Carbon Nanotubes as Gigahertz Oscillators. *Phys. Rev. Lett.* **88,** 045503 (2002).

33. Feldman, A.K., Steigerwald, M.L., Guo, X. & Nuckolls C. Molecular electronic devices based on single-walled carbon nanotube electrodes. *Acc. Chem. Res.* **41,** 1731-41 (2008).

34. Alberts B, Johnson A, Lewis J, Raff M, Roberts K, Walter P.*Molecular Biology of the Cell Ch. 4 Ed. 5th* (Garland Science, New York, 2002).

35. 34. van Holde, K.E., Johnson, W.C. and Ho, P.S. *Principles of Physical Biochemistry Ch. 1 Ed. 2* (Prentice Hall, New Jersey, 1998).

36. Gu, H., Chao, J., Xiao, S. & Seeman, N. C. Dynamic patterning programmed by DNA tiles captured on a DNA origami substrate. *Nat. Nanotechnol.* **4**, 245 - 248 (2009).

37. Seeman, N. C. DNA nanotechnology: novel DNA constructions. *Annu. Rev. Biophys. Biomol. Struct.* **27.** 225–248 (1998).

38. Chen, J. & Seeman, N. C. Synthesis from DNA of a molecule with the connectivity of a cube. *Nature* **350,** 631 633 (1991).

39. Ansari, A. A., Khan, M. N., Alhoshan, M., Aldwayyan, A. S. & Alsalhi, M. S. *Nanostructured materials: classification, properties, fabrication, characterization and their applications in biomedical sciences," in Nanoparticles: Properties,Classification, Characterization, and Fabrication* (Nova Science Publishers, Hauppauge, NY, USA, 2010).

40. Bath, J. & Turberfield, A. J. DNA nanomachines. *Nat. Nanotechnol.* **2,** 275 - 284 (2007).

41. Dittmer, W. U. & Simmel, F. C. Chains of semiconductor nanoparticles templated on DNA. *Appl. Phys. Lett.* **85,** 633–635 (2004).

42. Hahm, J.-I. & Lieber, C. M. Direct ultrasensitive electrical detection of DNA and DNA sequence variations using nanowire nanosensors. *Nano Lett.* **4,** 51–54 (2004).

43. Braun, E., Eichen, Y. Sivan, U. & Ben-Yoseph, G. DNAtemplated assembly and electrode attachment of a conducting silver wire *Nature* **391,** 775–778 (1998).

44. Dwyer, C. *et al.* DNA-functionalized single-walled carbon nanotubes. *Nanotechnology* 13, 601–604 (2002).

45. Hazani, M., Naaman, R., Hennrich, F. & Kappes, M. M. Confocal fluorescence imaging of DNA-functionalized carbon nanotubes. *Nano Lett.* **3,** 153–155 (2003).

46. Li, X., Peng, Y. & Qu, X. Carbon nanotubes selective destabilization of duplex and triplex DNA and inducing BA transition in solution. *Nucleic Acids Res.* **34,** 3670–3676 (2006).

47. Gao, H. & Kong, Y. Simulation of DNA nanotube interaction. *Annu. Rev. Mater. Res.* **34,** 123–150 (2004).

48. Singh, R. *et al.*, Binding and condensation of plasmid DNA onto functionalized carbon nanotubes: toward the construction of nanotube based gene delivery vectors. *J. Am. Chem. Soc.* **127,** 4388–4396 (2005).

49. Tu, X. & Zheng, M. A DNA-based Approach to the Carbon Nanotube Sorting Problem. *Nano Research* **1,** 185-194 (2008).

50. Rotkin, S. V. Electronic Properties of Nonideal Nanotube Materials: Helical Symmetry Breaking in DNA Hybrids. *Annu. Rev. Phys. Chem.* **61,** 241-261 (2009).

51. Tu, X., Manohar, S., Jagota, A. & Zheng, M. DNA sequence motifs for structure-specific recognition and separation of carbon nanotubes. *Nature* **460,** 250-253 (2009).

52. Kim, W. *et al.* Connecting Single Molecule Electrical Measurements to Ensemble Spectroscopic Properties for Quantification of Single-Walled Carbon Nanotube Separation. *J. Am. Chem. Soc.* **131,** 3128–3129 (2009).

53. Manohar, S. *et al.* Peeling Single-Stranded DNA from Graphite Surface to Determine Oligonucleotide Binding Energy by Force Spectroscopy *Nano Lett.* **8,** 4365-4372 (2008).

54. Albertorio, F., Hughes, M., Golovchenko, J. & Branton, D. Base dependent DNA–carbon nanotube interactions: activation enthalpies and assembly–disassembly control. *Nanotechnology* **20,** (2009).

55. Manohar, S., Tang, T. & Jagota, A. Structure of Homopolymer DNA-CNT Hybrids. *J. Phys. Chem. C* **111,** 17835–17845 (2007).

56. Martin, W., Zhu, W. & Krilov, G. Simulation Study of Noncovalent Hybridization of Carbon Nanotubes by Single Stranded DNA in Water. *J. Phys. Chem. B* **112,** 16076–16089 (2008).

57. Johnson, R.R., Johnson, A. T. C. & Klein, M. L. Probing the Structure of DNA-Carbon Nanotube Hybrids with Molecular Dynamics. *Nano Lett.* **8,** 69–75 (2008).

58. Abdula, D., Nguyen, K. T. & Shim, M., Raman Spectral Evolution in Individual Metallic Single-Walled Carbon Nanotubes upon Covalent Bond Formation. *J. Phys. Chem. C* **111**, 17755 (2007).

59. Zhang, L. *et al.* Assessment of Chemically Separated Carbon Nanotubes for Nanoelectronics. *J. Am. Chem. Soc.* **130,** 2686–2691 (2008).

60. Sivasankar, B. *Bioseparations: Principles and Techniques. Ch.9* (Prentice-hall Of India Pvt Ltd, Delhi, 2005).

61. Senapati, M.R. *Advanced Engineering Chemistry Ch. 2 Ed. 2.* (Laxmi Publications (P) LTD. Daryaganj, New delhi, 2006).

62. Lin, M. F. Optical spectra of single-wall carbon nanotube bundles. *Phys. Rev. B* **62,** 153-159 (2000).

63. Huang,L. *et al.* A Generalized Method for Evaluating the Metallic-to-Semiconducting Ratio of Separated Single-Walled Carbon Nanotubes by UV-vis-NIR Characterization. *J. Phys. Chem. C* **114,** 12095–12098 (2010).

64. Samsonidze, Ge. G., Family behavior of the optical transition energies in single-wall carbon nanotubes of smaller diameters. *Appl. Phys. Lett.***85,** 5703-5705 (2004).

65. Zhang, L. *et al.* Optical Characterizations and Electronic Devices of Nearly Pure (10,5) Single-Walled Carbon Nanotubes. *J. Am. Chem. Soc.* **131,** 2454–2455 (2009).

66. Abramovitch, D. Y., Andersson, S. B., Pao, L. Y. and Schitter. G., *A Tutorial on the Mechanisms, Dynamics, and Control of Atomic Force Microscopes* (Proc. American Control Conf., New York, 2007).

67. Schönherr, H., Vancso, G. J., *Scanning Force Microscopy of Polymers* (Springer, 2010).

68. Wei Lu & Charles M. Lieber. Nanoelectronics from the bottom up. *Nat. Mater.* **6,** 841 – 850 (2007).

69. McEuen, P. L., Fuhrer, M. S. & Park, H. Single-walled carbon nanotube electronics. *IEEE Trans. Nanotechnol.* **1,** 78–85 (2002).

70. Lieber, C. M. Nanoscale science and technology: building a big future from small things. *Mater. Res. Soc. Bull.* **28,** 486–491 (2003).